Cooperative Multi-Satellite and Multi-RIS Beamforming: Enhancing LEO SatCom and Mitigating LEO-GEO Intersystem Interference

Ziyuan Zheng, *Graduate Student Member, IEEE,* Wenpeng Jing, Zhaoming Lu, Qingqing Wu, *Senior Member, IEEE,* Haijun Zhang, *Fellow, IEEE,* and David Gesbert, *Fellow, IEEE*

***Abstract*—Satellite communication (SatCom) is regarded as a key enabler for bridging connectivity and capacity gaps in sixth-generation (6G) networks. However, the proliferation of Low Earth Orbit (LEO) satellites raises significant intersystem interference risks with Geostationary Earth Orbit (GEO) systems. This paper introduces a cooperative multi-satellite multi-reconfigurable intelligent surface (RIS) transmission framework to mitigate such interference while enhancing LEO SatCom performance. Specifically, cooperative beamforming is designed under a non-coherent cell-free paradigm, considering both adaptive and max ratio (MR) precoding, as well as statistical and two-timescale channel state information (CSI), aiming to synthesize the advantages of cell-free and RIS into SatCom in a practical way. Firstly, an alternating optimization (AO)-based design leveraging statistical CSI with adaptive precoding is proposed. Then, we propose a power allocation algorithm under MR precoding with given RIS phase shifts obtained from the former, along with a direct two-stage design bypassing prior results. Additionally, we extend derived closed-form expressions and proposed algorithms to exploit two-timescale CSI. Numerical results demonstrate the impact of intersystem interference mitigation constraints, compare the performance of proposed algorithms, draw insights into the effects of transmit power, interference threshold, and Rician factors, validate SatCom performance enhancements achieved by RISs, and discuss the advantages of multi-satellite cooperation.**

***Index Terms*—reconfigurable intelligent surface, Low Earth Orbit satellite communication, cooperative beamforming, co-frequency interference mitigation, multi-satellite cooperation.**

I. Introduction

While the terrestrial fifth-generation (5G) system has been deployed and operated, capacity gaps remain in sparsely populated and geographically isolated areas. In this context, satellite communication (SatCom) is regarded as a key enabler to provide ubiquitous connectivity and capacity in-fill in the future sixth-generation (6G) blueprint [1]. According to different orbital altitudes, two major types of SatCom systems are Geostationary Earth Orbit (GEO) and Low Earth Orbit (LEO) systems. GEO satellites, positioned approximately 36,000 kilometers above the Earth's equator, remain stationary relative to the Earth's surface, providing coverage over vast regions. Conversely, LEO satellites operate at lower altitudes and fast speeds, covering smaller areas but offering lower latency and higher capacity. In recent years, the mature manufacturing and launch process has led to a rejuvenation in LEO SatCom constellations [2]. Formed by mega-scale nodes in space, LEO constellations are expected to provide seamless coverage and broadband interactive data services.

However, the development and deployment of SatCom systems are driving a proliferation of active LEO satellites. For instance, SpaceX's Ku and Ka-band constellation is projected to include approximately 12,000 LEO satellites in its initial phase, potentially expanding to 42,000 satellites [3], and over 5,600 of them have already operated in orbit. This ever-increasing number raises concerns about potential harmful intersystem interference between LEO and GEO systems. Such interference may degrade communication performance or cause failure in GEO systems due to their fixed position and severe path loss [4]. Among the various interference types, co-frequency interference is a primary concern, occurring when different systems share the same frequency band. Particularly, when an active LEO satellite passes through the line-of-sight path between an Earth station and its corresponding GEO satellite, the GEO system may suffer overwhelmed downlink interference, termed as *in-line* events by the International Telecommunication Union (ITU) [5].

To avoid severe interference events like *in-line* events, ITU has established strict standards for interference avoidance on GEO satellites operating under LEO-GEO spectrum sharing scenarios [6]. Therefore, various techniques have been devised for this imperative intersystem interference mitigation requirement. In the *frequency domain*, interference coordination and frequency allocation can be performed when satellite systems are cooperative. Alternatively, cognitive radio (CR) technologies enable dynamic spectrum sharing over co-frequency LEO and GEO systems [7]. In the *power domain*, controlling transmit power to satisfy interference protection constraints for GEO terminals (GTs) is a direct approach, which can be cognitive or non-cognitive, typically combined with modulation and coding adaption to maintain LEO system availability

Z. Zheng, W. Jing, and Z. Lu are with the Beijing Laboratory of Advanced Information Networks, Beijing University of Posts and Telecommunications, 100083, China (e-mail: ziyuanzheng@bupt.edu.cn; jingwenpeng@bupt.edu.cn; lzy0372@bupt.edu.cn).

Q. Wu is with the Department of Electronic Engineering, Shanghai Jiao Tong University, 200240, China (e-mail: qingqingwu@sjtu.edu.cn).

H. Zhang is with the School of Computer & Communication Engineering, University of Science and Technology Beijing, 100083, China (e-mail: zhanghaijun@ustb.edu.cn).

D. Gesbert is with the Department of Communications Systems, EURECOM, 06904 Sophia Antipolis, France (e-mail: david.gesbert@eurecom.fr).

Z. Zheng, W. Jing, and Z. Lus' work is supported by the Beijing Natural Science Foundation (BNSF) under Grant L222003; Q. Wu's work is supported by NSFC 62371289 and NSFC 62331022.

This article has been presented in part at the IEEE Wireless Communications and Networking Conference (WCNC) 2024 [1].

[8]. In th *Spatial domain*, initially, for satellites with a single wide beam, the ITU recommends spatial isolation based on link separation or exclusion angles. Subsequently, a side-look strategy using beam sidelobes for communication ensures LEO system availability by leveraging satellite diversity [9].

Recently, with the application of advanced antenna techniques like phased arrays, high-throughput multibeam satellite systems (MSSs) with flexible beam coverage have become prevalent in the new space era, promoting beam hopping and satellite precoding to emerge as current research hotspots [10]. Through proper design, these multibeam techniques can also be utilized to develop *'evolved' spatial domain* strategies for intersystem interference mitigation [11]. Among MSSs, the precoded MSS with full frequency reuse (FFR) stands out for superior communication potential, considered one of the most promising choices for next-generation SatCom systems. Specifically, the downlink, i.e, forward link, part in a precoded MSS represents a multiuser multiple-input multiple-output (MIMO) system, efficiently utilizing available bandwidth over sufficiently separated beams while maintaining a low multiuser interference [12]. Existing research studies various precoding designs with practical constraints in SatCom [13].

The evolution of MIMO technology in precoding MSSs mirrors cellular massive MIMO (mMIMO) and cell-free systems in terrestrial networks, progressing in two directions: centralized/single-satellite mMIMO and distributed/multi-satellite cooperative transmission. A mMIMO channel model and transmission scheme for LEO SatCom is proposed with statistical CSI-based precoding and receiving [14]. Then, for planar array user terminals, the rank-one channel matrix makes single-stream precoding optimal for maximizing system throughput [16]. Similar to cell-free systems, multi-satellite cooperation transmission offers high spectral efficiency due to spatial diversity [17]. Particularly, in LEO-GEO coexistence scenarios, LEO systems can leverage satellite diversity and beamforming gain to improve communication performance and mitigate intersystem interference. Nevertheless, synchronization between satellites may hinder the practicality of cooperation. A position-based precoding and receive equalizer designs for multi-antenna ground stations in a LEO multi-satellite system is proposed in [18] without addessing synchronization issues. To tackle time-frequency asynchrony, a spatial linear receiver method is introduced in [19]. In addition, hybrid beamforming multi-satellite transmission frameworks with user scheduling can be utilized for reducing complexity and power consumption [15]. However, to ensure favorable performance, applying a cell-free paradigm in SatCom requires large-scale satellite deployment and substantial hardware and power expenses [20]. This poses challenges due to severe path loss in satellite links and fewer satellites compared to terrestrial cell-free systems, potentially resulting in unsatisfactory energy efficiency or received signal strength.

Fortunately, reconfigurable intelligent surface (RIS), a disruptive technique springing up in wireless communications, has been deemed a solution to the above problems [21]. Specifically, through passive beamforming via element-wise phase shift designs at the RIS, favorable reflecting paths can be introduced to enhance received power and spectral efficiency for existing wireless systems [22]. Notably, since RIS does not require extra hardware implementation, its integration into cell-free systems can enhance performance with low cost and power consumption [23]. Research on RIS-aided cell-free systems has demonstrated improvements in capacity and energy efficiency [24]. Similarly, by incorporating RIS in ground segments with properly designed phase shifts, multi-satellite cooperation SatCom systems can benefit from improved link budget and signal processing capability. Particularly in LEO-GEO spectrum sharing scenarios, RIS can compensate for performance losses caused by LEO-GEO interference mitigation, thereby improving the availability of the LEO system. To the authors' knowledge, although some studies have investigated RIS-aided SatCom for relaying in blockage scenario [25]-[27], improving the signal-to-noise ratio [28],[29], physical layer security [30]-[33], covert communication [34],[35], and satellite-ground integrated/relay networks [36]-[38], literature on exploring this multi-satellite multi-RIS cooperative framework remains limited.

From a technical perspective, cooperative beamforming in RIS-aided cell-free systems have utilized various types of CSI [39], including instantaneous [24], pure statistical [40]-[42], and two-timescale CSI [43]. Pure statistical are practical due to its lower channel estimation overhead requirement. Specifically, [40] provides closed-form approximations for achievable rates of RIS-assisted mMIMO systems under the Rician channel and statistical CSI, allowing joint power control and phase shift design to maximize the ergodic capacity of multi-user and multi-cell MISO systems [41],[42]. To reduce channel estimation overhead while retaining performance gains, the two-timescale transmission protocol is introduced into RIS-assisted wireless systems by using slow-varying statistical CSI for RIS passive beamforming and instantaneous superimposed CSI for active beamforming [43]. Generally, adaptive precoding and max ratio (MR) precoding are considered, with the former offering higher optimization flexibility and the latter reducing system overhead and effectively exploiting two-timescale CSI [23]. However, specific characteristics of SatCom are not accounted for. Firstly, existing works typically assume coherent transmission, requiring perfect synchronization between transmitters, which is unrealistic in SatCom systems. Secondly,the LEO-GEO intersystem interference is quite likely to occur, due to the natural broadcasting characteristics, yet mitigating this interference is not addressed. Lastly, fairness, an important metric in SatCom, is ignored in many existing studies, which primarily focus on improving sum rates.

Motivated by the observations above, this paper investigates RIS-aided LEO SatCom with LEO-GEO intersystem interference mitigation. Specifically, the system explores the cooperative operation of multiple LEO satellites in the space segments and multiple RISs in the ground segments, employing jointly designed active and passive beamforming to enhance SatCom performance within a non-coherent cell-free MIMO paradigm while suppressing LEO-GEO co-frequency interference. The main contributions of this paper can be summarized as follows:

- First, we formulate cooperative beamforming optimization problems considering adaptive and MR precoding, as well as statistical and two-timescale CSI under a non-

coherent cell-free paradigm to synthesize the advantages of cell-free and RIS into SatCom in a practical way.

- Second, we propose an alternating optimization (AO)-based cooperative beamforming design leveraging pure statistical CSI with adaptive precoding, resorting to fractional programming and manifold optimization methods.
- Third, we propose a cooperative beamforming design under MR precoding, where a closed-form optimization problem is derived, and power allocation is performed with given RIS phase shifts obtained from the adaptive-precoding case.
- Fourth, we propose a two-stage design under MR precoding that does not require adaptive precoding results. Here, we develop an iterative algorithm for RIS phase shift optimization using exponential smoothing, sum-square penalty, and manifold optimization techniques.
- Last, we extend closed-form expressions and proposed algorithms for cooperative beamforming exploiting two-timescale CSI, i.e., instantaneous CSI at LEO satellites and statistical CSI at RISs.

In the following, Section II introduces the system model and problem formulation. Section III presents the AO-based algorithm exploiting statistical CSI and adaptive precoding. Section IV proposes a power allocation design precoding using given RIS phase shifts, and Section V outlines the two-stage design under MR precoding. Section VI extends the algorithms to exploit two-timescale CSI, followed by numerical results in Section VII and conclusions in Section VIII.

Notations: Scalars are denoted by italic letters, and vectors and matrices are denoted by bold-face lower and upper-case letters, respectively. $\mathbb{C}^{x\times y}$ denotes the space of complex matrices. For a complex-valued scalar x, $|x|$ denotes its modulus. For a complex-valued vector $\boldsymbol{x}$, $\|\boldsymbol{x}\|$ denotes its Euclidean norm, $\boldsymbol{x}^{\dagger}$ denotes its conjugate, and $\mathrm{diag}\,(\boldsymbol{x})$ denotes a diagonal matrix with each diagonal element being the element in $\boldsymbol{x}$. The distribution of a circularly symmetric complex Gaussian random vector with mean vector $\boldsymbol{x}$ and covariance matrix $\boldsymbol{\Sigma}$ is denoted by $\mathcal{CN}\,(\boldsymbol{x},\boldsymbol{\Sigma})$. The Euclidean gradient of a scalar function $f(\boldsymbol{x})$ with a vector variable $\boldsymbol{x}$ is denoted by $\nabla f(\boldsymbol{x})$. For a square matrix $\boldsymbol{S}$, $\mathrm{tr}\,(\boldsymbol{S})$ denote its trace. For any general matrix, $\boldsymbol{M}^{H}$, $\mathrm{rank}\,(\boldsymbol{M})$, and $[\boldsymbol{M}]_{i,j}$ denote its conjugate transpose, rank, and (i,j)th element,respectively. $\boldsymbol{I}$ and $\boldsymbol{0}$ denote an identity and an all-zero matrix, respectively. $\mathrm{Re}(\cdot)$ denote the real part of a complex number. $\odot$ denotes the Hadamard product. $\mathbb{E}(\cdot)$ stands for the expectation operation.

II. System Model and Problem Formulation

As illustrated in Fig. 1, we consider a LEO and GEO spectrum-sharing scenario. J multibeam LEO satellites, each equipped with $N = N_r \times N_c$ uniform planar array (UPA) transmit antennas, operate cooperatively to provide unicast services to U fixed single antenna LEO users (LUs). The single antenna assumption for terminals is made to clarify the fundamental behavior of our proposed schemes and aligns with many existing works in SatCom, cell-free, and RIS-aided systems [13],[14],[17],[20],[23],[24]. While the multi-antenna terminal configuration is more generalized and used in some works to enhance SatCom performance, our focus is on the proposed RIS-aided multi-satellite transmission scheme, and its extension to include multi-antenna terminals will be addressed in future work. To improve spectral efficiency, the LEO satellites adopt FFR and employ linear precoding to mitigate intrasystem inter-beam interference and LEO-GEO intersystem interference. Simultaneously, the GEO satellite uses the same frequency band, delivering broadcasting services to K fixed GTs.

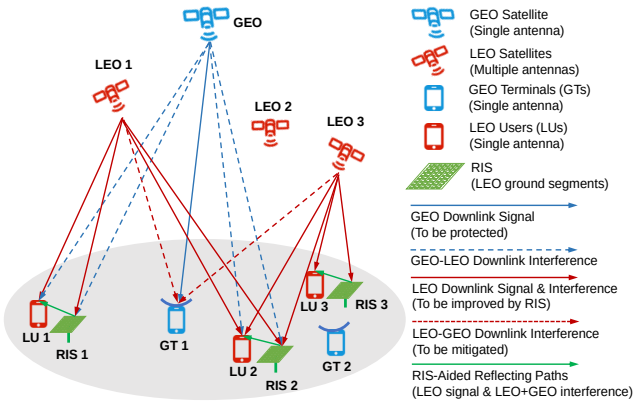

Fig. 1. Multi-satellite multi-RIS LEO-GEO spectrum-sharing systems.

To enhance LEO SatCom performance, U distributed RISs are employed around each LU in the ground segments. Each RIS consists of $M = M_r \times M_c$ reflecting subsurfaces, and each subsurface comprises a number of adjacent elements inducing an identical phase shift to incident signals for high aperture gain. We assume the RISs are cooperatively controlled via onboard processing through reliable backhaul links. Each RIS reflects signals primarily to its specified adjacent LU, which corresponds to a user-specific deployment referred to as [44]. The coverage area of a satellite beam is significantly larger than that of a terrestrial cellular network, leading to considerable geographical distances between simultaneously scheduled users [12]. Given the multiplicative path loss nature of the RIS, the reflected signals from a RIS to non-dedicated users in different beams are almost negligible [45]. In satellite communication scenarios, RISs can be strategically deployed on the ground to cover a large service area with T ground users. We consider a subset of U users at any given time, where U is the number of available RISs. Different sets of U users from the total T users are served in different time slots, eliminating the need to deploy as many RISs as total users. This strategy is both economically feasible and practical, effectively serving multiple users over time with a manageable number of RISs

A. Channel Model

Denote the set of LUs, GTs, and LEO satellites as $\mathcal{U} = \{1,\ldots,U\}$, $\mathcal{K} = \{1,\ldots,K\}$, and $\mathcal{J} = \{1,\ldots,J\}$, respectively. We model the channels of satellite-to-ground and RIS-enabled reflecting links. For the sake of illustration, we use LEO systems as an example. To describe the channel with a strong line-of-sight (LoS) path, the Rician fading model is adopted for all channels involved. Specifically, the equivalent baseband channels from j-th LEO satellite to u-th RIS, from

j-th satellite to u-th LU, and from a RIS to its adjacent LU are denoted by $\boldsymbol{G}_{LR,ju} \in \mathbb{C}^{N\times M}, \boldsymbol{h}_{LL,ju} \in \mathbb{C}^{N\times 1}$, and $\boldsymbol{h}_{R,u} \in \mathbb{C}^{M\times 1}$, respectively, as follow

$$\boldsymbol{h}_{LL,ju}= \sqrt{\frac{\mu_{LL,ju}}{1+\kappa_{LL,ju}}}\left(\sqrt{\kappa_{LL,ju}}\bar{\boldsymbol{h}}_{LL,ju}+\tilde{\boldsymbol{h}}_{LL,ju}\right), \quad (1a)$$

$$\boldsymbol{h}_{R,u} = \sqrt{\frac{\mu_{R,u}}{1+\kappa_{R,u}}}\left(\sqrt{\kappa_{R,u}}\bar{\boldsymbol{h}}_{R,u}+\tilde{\boldsymbol{h}}_{R,u}\right), \quad (1b)$$

$$\boldsymbol{G}_{LR,ju} = \sqrt{\frac{\mu_{LR,ju}}{1+\kappa_{LR,ju}}}\left(\sqrt{\kappa_{ju}}\bar{\boldsymbol{G}}_{LR,ju}+\tilde{\boldsymbol{G}}_{LR,ju}\right), \quad (1c)$$

where $\kappa_{LL,ju}$, $\kappa_{R,u}$ and $\kappa_{LR,ju}$ are Rician factors, $\mu_{LL,ju}$, $\mu_{R,u}$, and $\mu_{LR,ju}$ are the large-scale path-loss coefficient between the satellite and LUs, the RIS and LUs, and the satellite and the RIS, respectively. $\bar{\boldsymbol{h}}_{LL,ju}$, $\bar{\boldsymbol{h}}_{R,u}$, and $\bar{\boldsymbol{G}}_{LR,ju}$ are normalized phase-only LoS components of corresponding channels, which can be readily obtained from space angle or position information [23]. Specifically, for j-th LEO satellite and u-th LU, we denote the array response of UPAs $\bar{\boldsymbol{G}}_{LR,ju} = \mathbf{a}_M^T(\vartheta_{AoA1,ju},\psi_{AoA1,ju})\,\mathbf{a}_N(\vartheta_{AoD,ju},\psi_{AoD,ju})$, $\bar{\boldsymbol{h}}_{R,u} = \mathbf{a}_M^T(\vartheta_{AoA2,u},\psi_{AoA2,u})$, and $\bar{\boldsymbol{h}}_{LL,ju} = \mathbf{a}_N^T(\vartheta_{AoA3,ju},\psi_{AoA3,ju})$, where $\vartheta_{AoA1,ju}$ and $\vartheta_{AoA2,ju}$ are the azimuth angles of arrival (AoA) to the u-th RIS, and $\psi_{AoA1,ju}$ and $\psi_{AoA2,ju}$ are the elevation AoAs to the u-th RIS, $\vartheta_{AoA3,ju}$ and $\psi_{AoA3,ju}$ are the azimuth and elevation AoA to the j-th satellite, respectively, and $\vartheta_{AoD,ju}$ and $\psi_{AoD,ju}$ are the azimuth and elevation angle of departure (AoD) form the j-th satellite, respectively [20]. Besides, $\mathbf{a}_N(\vartheta,\psi) = [1,\ldots,e^{j2\pi\frac{d_1}{\lambda}(n_r\cos(\vartheta)\sin(\psi)+n_c\sin(\vartheta)\sin(\psi))},\ldots,e^{j2\pi\frac{d_1}{\lambda}((N_r-1)\cos(\vartheta)\sin(\psi)+(N_c-1)\sin(\vartheta)\sin(\psi))}]$ and $\mathbf{a}_M(\vartheta,\psi)=[1,\ldots,e^{j2\pi\frac{d_2}{\lambda}(m_r\cos(\vartheta)\sin(\psi)+m_c\sin(\vartheta)\sin(\psi))},\ldots,e^{j2\pi\frac{d_2}{\lambda}((M_r-1)\cos(\vartheta)\sin(\psi)+(M_c-1)\sin(\vartheta)\sin(\psi))}]$ are the array response with d_1 being the satellite antenna spacing and d_2 being the RIS elements spacing, and λ is the wavelength. On the other hand, $\tilde{\boldsymbol{h}}_{LL,ju}$, $\tilde{\boldsymbol{h}}_{R,u}$, and $\tilde{\boldsymbol{G}}_{LR,ju}$ are the NLoS Rayleigh components, which are independently and identically distributed complex Gaussian random variables with zero mean and unit variance. Note that spatial correlation on the antenna arrays can be incorporated into the LoS components, and thus, the NLoS components are modeled by independent Rayleigh random variables. Following with a similar process to (1), the channels from the GEO satellite to RIS, LUs, and GTs and from the LEO satellite to GTs can be modeled as $\boldsymbol{g}_{GR,u}^T \in \mathbb{C}^{M\times 1}, h_{GL,u}$, $h_{GG,k}$, and $\boldsymbol{h}_{LG,jk} \in \mathbb{C}^{N\times 1}$, respectively. Here, the details are omitted for brevity.

B. Downlink Transmission Signal Model

The received signals are a combination of direct and RIS-aided cascaded signals. Let $\boldsymbol{W} = [\boldsymbol{W}_1,\cdots,\boldsymbol{W}_J]^H \in \mathbb{C}^{NJ\times U}$ denote the linear precoding matrices at LEO satellites. Each satellite's specific precoding matrix is $\boldsymbol{W}_j$, i.e., $\boldsymbol{W}_j = [\boldsymbol{w}_{j1},\cdots,\boldsymbol{w}_{jU}]$, and each user is assigned one dedicated beamforming vector from a satellite. The complex baseband transmitted signal sent by j-th satellite can be expressed as $\boldsymbol{x}_j = \boldsymbol{W}_j\boldsymbol{s}_j$, where $\boldsymbol{s} = [s_{j1},\cdots,s_{jU}]^T$ denotes data vector with zero-mean and normalized-power independent variables. Let $\boldsymbol{\phi}_u = [\phi_{u,1},\cdots,\phi_{u,M}]$ denote the reflection coefficients of u-th RIS, where the reflection amplitudes of all elements are set to the maximum value one to maximize the signal reflection power, i.e., $|\phi_{u,m}| = 1, \forall m$. $\boldsymbol{\Phi}_u = \mathrm{diag}(\boldsymbol{\phi}_u)$ represents the a RIS's diagonal reflection matrix, and $\boldsymbol{\Phi} = [\boldsymbol{\Phi}_1,\cdots,\boldsymbol{\Phi}_U]$ represents for all RIS phase shiftes involved.

The cooperative multi-satellite transmission framework is similar to the *cell-free MIMO* paradigm [17]. To draw insights on the optimal performance gain and for the convenience of controlling RISs, we consider the fully centralized processing where all signals are processed in the head of the LEO satellites. To avoid the unrealistic assumption that perfect synchronization is performed between LEO satellites, we consider the non-coherent transmission pattern, where each LEO satellite transmits independent signals separately received and decoded by LUs [17]. Then, combining multi-RIS, we describe the downlink transmission signal model. With the aid of its corresponding RIS, the superimposed signal received at the u-th LU can be expressed as

$$y_u = \underbrace{\sum\nolimits_{j\in\mathcal{J}}(\boldsymbol{h}_{LL,ju}^H + \boldsymbol{h}_{R,u}^H\boldsymbol{\Phi}_u^H\boldsymbol{G}_{LR,ju}^H)\boldsymbol{w}_{ju}s_u}_{\text{Useful Signals from LEO Satellites}} \quad (2a)$$

$$+ \underbrace{\sum\nolimits_{j\in\mathcal{J}}(\boldsymbol{h}_{LL,ju}^H + \boldsymbol{h}_{R,u}^H\boldsymbol{\Phi}_u^H\boldsymbol{G}_{LR,ju}^H)\sum\nolimits_{i\in\mathcal{U},i\neq u}\boldsymbol{w}_{iu}s_i}_{\text{Intrasystem Interference from LEO Satellites}} \quad (2b)$$

$$+ \underbrace{(h_{GL,u}^H + \boldsymbol{h}_{R,u}^H\boldsymbol{\Phi}_u^H\boldsymbol{g}_{LR,u}^\dagger)s_0}_{\text{Intersystem Interference from the GEO Satellite}} + n_u, \quad (2c)$$

where $n_u \sim \mathcal{CN}(0,\sigma^2)$ denotes the additive white Gaussian noise (AWGN) at the user's receiver. Similarly, the received signal at k-th GT can be expressed as

$$y_k = \underbrace{h_{GG,k}^\dagger s_0}_{\text{GEO Signal}} + \underbrace{\sum\nolimits_{j\in\mathcal{J}}\sum\nolimits_{u\in\mathcal{U}}\boldsymbol{h}_{LG,jk}^H\boldsymbol{w}_{ju}s_u}_{\text{LEO}-\text{GEO Intersystem Interference}} + n_k. \quad (3)$$

To reap substantial performance gains under non-coherent multi-satellite cooperation, we consider successive interference cancellation (SIC) receivers for LUs. For a general non-coherent cell-free paradigm without RISs and GEO satellite, when u-th LU detects received signals using SIC with arbitrary decoding order, a lower bound of signal-to-interference-plus-noise (SINR) can be given by

$$\mathrm{SINR}_u^{\mathrm{LB}} = \frac{\sum_{j=1}^J\left|\mathbb{E}\{\boldsymbol{h}_{ju}^H\boldsymbol{w}_{ju}\}\right|^2}{\sum_{j=1}^J\sum_{i=1}^U\mathbb{E}\{\left|\boldsymbol{h}_{ju}^H\boldsymbol{w}_{ji}\right|^2\}-\sum_{j=1}^J\left|\mathbb{E}\{\boldsymbol{h}_{ju}^H\boldsymbol{w}_{ju}\}\right|^2+\sigma_u^2}. \quad (4)$$

Proof: See Appendix A. ■

Note that the non-coherent transmission yields inferior performance compared to coherent transmission with a larger signal term. However, to achieve the coherent beamforming gain, coherent transmission requires synchronizing all transmitters, which is impractical in SatCom scenarios.

C. Problem Formulation

In this research, we aim to improve the performance of LEO SatCom under the LEO-GEO interference mitigation constraint. We achieve this by jointly optimizing the precoding

$$\mathrm{SINR}_u^{\mathrm{sCSI,AP}} = \sum_{j\in\mathcal{J}} \left|\mathbb{E}\Big\{\Big(\boldsymbol{h}_{LL,ju}^H + \boldsymbol{h}_{R,u}^H\boldsymbol{\Phi}_u^H\boldsymbol{G}_{LR,ju}^H\Big)\boldsymbol{w}_{ju}\Big\}\right|^2 \Bigg(\sum_{j\in\mathcal{J}}\sum_{i\in\mathcal{U}} \mathbb{E}\Big\{\left|\Big(\boldsymbol{h}_{LL,ju}^H + \boldsymbol{h}_{R,u}^H\boldsymbol{\Phi}_u^H\boldsymbol{G}_{LR,ju}^H\Big)\boldsymbol{w}_{ji}\right|^2\Big\} - \sum_{j\in\mathcal{J}}\left|\mathbb{E}\left\{\left(\boldsymbol{h}_{LL,ju}^H + \boldsymbol{h}_{R,u}^H\boldsymbol{\Phi}_u^H\boldsymbol{G}_{LR,ju}^H\right)\boldsymbol{w}_{ju}\right\}\right|^2 + \left|h_{GL,u}^H + \boldsymbol{h}_{R,u}^H\boldsymbol{\Phi}_u^H\boldsymbol{g}_{GR,u}^\dagger\right|^2 + \sigma_u^2\Bigg)^{-1} \tag{5}$$

at LEO satellites and the reflective beamforming at RISs. According to (4), we can only use statistical CSI to design cooperative beamforming. In fact, two-timescale CSI can be leveraged under the MR precoding case. Nevertheless, with general adaptive precoding, the SINR of each LU's received signal can be shown in (5) at the top of the next page.

Besides, to illustrate the impact of intersystem interference, we express the SINR of GTs as follows

$$\mathrm{SINR}_k = \frac{|h_{GG,k}^\dagger|^2}{\sum_{j\in\mathcal{J}}\sum_{u\in\mathcal{U}}|\boldsymbol{h}_{LG,jk}^H\boldsymbol{w}_{ju}|^2 + \sigma_k^2}. \tag{6}$$

Because instantaneous CSI can not be exploited, we use the average aggregate LEO-GEO inter-system interference for system design, which is required to be below a threshold ς_k.

$$\sum_{j\in\mathcal{J}}\sum_{u\in\mathcal{U}}\mathbb{E}\Big\{\left|\boldsymbol{h}_{LG,jk}^H\boldsymbol{w}_{ju}\right|^2\Big\} \le \varsigma_k, \forall k\in\mathcal{K}, \tag{7}$$

As fairness over users is an important performance metric in SatCom, we take minimum SINR as the objective function to maximize. The optimization problem can be formulated as

$$\begin{aligned}
(\mathrm{P1}): \max_{\{\boldsymbol{\Phi}_u\}_{u=1}^U, \boldsymbol{W}} \ & \min_{\forall u\in\mathcal{U}} \ \left\{\mathrm{SINR}_u^{\mathrm{sCSI}}\right\} && \text{(8a)}\\
\text{s.t.} \ & \textstyle\sum_{u\in\mathcal{U}}\|\boldsymbol{w}_{ju}\|^2 \le P_T, \forall j\in\mathcal{J}, && \text{(8b)}\\
& |\phi_{u,m}|^2 = 1, \forall u\in\mathcal{U}, \forall m, && \text{(8c)}\\
& (7), &&
\end{aligned}$$

where P_T in (8b) is the maximum total beam power supported by the power amplifier on the LEO satellite, (7) is the aforementioned LEO-GEO intersystem interference mitigation constraint, and (8c) is the unit-modulus constraint on passive RIS phase shifters. It is challenging to solve (P1) due to 1) implicit-form expressions on optimization variables with expectation operation, 2) the non-concave fractional SINR expressions in the objective function, 3) the coupled non-convex transmit precoding and RIS phase shifts optimization variables, and 4) the non-convex quadratic unit-modulus constraints at phase shifters of the RIS. Generally, there is no standard method for optimally solving such non-convex optimization problems.

III. Cooperative Beamforming Design Exploiting Statistical CSI with Adaptive Precoding

In this section, we consider optimal adaptive precoding, which allows $\boldsymbol{W}$ to be designed arbitrarily without structural constraints like MR precoding. To efficiently solve (P1) with coupled variables, we split (P1) into satellite precoding and RIS passive beamforming subproblems by resorting to the AO method. Additionally, we resort to fractional programming and manifold optimization techniques to tackle the subproblems.

A. Satellite Active Beamforming

For the satellite precoding optimization subproblem with given $\boldsymbol{\Phi}_u, \forall u\in\mathcal{U}$, the non-convex minimum SINR maximization objective function (8a) is just subject to a convex total beam power constraint (8b) and an equivalent signal power threshold constraint (7). Then, by introducing an auxiliary variable γ, we can rewritten the subproblem into (P2) as follow

$$\begin{aligned}
(\mathrm{P2}): \max_{\{\boldsymbol{\Phi}_u\}_{u=1}^U, \boldsymbol{W}, \gamma} \ & \gamma && \text{(9a)}\\
\text{s.t.} \ & \mathrm{SINR}_{\mathrm{u}}^{\mathrm{sCSI,AP}} \ge \gamma, \forall u\in\mathcal{U}, && \text{(9b)}\\
& \textstyle\sum_{j\in\mathcal{J}}\sum_{u\in\mathcal{U}}\boldsymbol{w}_{ju}^H\boldsymbol{\Psi}_{jk}\boldsymbol{w}_{ju} \le \varsigma_k, \forall k\in\mathcal{K}, && \text{(9c)}\\
& (8b), &&
\end{aligned}$$

where $\mathrm{SINR}_{\mathrm{u}}^{\mathrm{sCSI,AP,CF}}$ is written in (10) with closed-form expressions at the top of this page after calculating expectation terms in (5), and $\boldsymbol{\Theta}_{ju}$, $\boldsymbol{\Xi}_{ju}$, and $f_1(\boldsymbol{\Phi}_u)$ are written as

$$\begin{aligned}
\boldsymbol{\Theta}_{ju} &= \alpha_{R,u}^2\alpha_{LR,ju}^2\bar{\boldsymbol{R}}_{LL,ju}\boldsymbol{\phi}_u\boldsymbol{\phi}_u^H\bar{\boldsymbol{R}}_{LL,ju}^H \\
&+ \alpha_{LL,ju}\alpha_{R,u}\alpha_{LR,ju}(\bar{\boldsymbol{R}}_{LL,ju}\boldsymbol{\phi}_u\bar{\boldsymbol{h}}_{LL,ju}^H + \bar{\boldsymbol{h}}_{LL,ju}\boldsymbol{\phi}_u^H\bar{\boldsymbol{R}}_{LL,ju}^H) \\
&+ \alpha_{LL,ju}^2\bar{\boldsymbol{h}}_{LL,ju}\bar{\boldsymbol{h}}_{LL,ju}^H && \text{(11a)}\\
\boldsymbol{\Xi}_{ju} &= \boldsymbol{\Theta}_{ju} + (\beta_{LL,ju}^2 + \beta_{LR,ju}^2\mu_{R,u}M)\boldsymbol{I}_N \\
&+ \alpha_{LR,ju}^2\beta_{R,u}^2\bar{\boldsymbol{G}}_{LR,ju}\bar{\boldsymbol{G}}_{LR,ju}^H, && \text{(11b)}\\
f_1(\boldsymbol{\Phi}_u) &= (\alpha_{GL,ju}\alpha_{R,u}\alpha_{GR,u} + \alpha_{GR,u}^2\alpha_{R,u}^2)\|\bar{\boldsymbol{r}}_{GL,ju}\boldsymbol{\phi}_u\|^2 \\
&+ (\beta_{GL,ju}^2 + \beta_{GR,ju}^2\mu_{R,u}M) + (\alpha_{GL,ju}^2 + \alpha_{GR,u}^2\beta_{R,u}^2M), && \text{(11c)}
\end{aligned}$$

where we denote large-scale channel statistics for brevity by letting $\alpha_{LL,ju} = \sqrt{\frac{\mu_{LL,ju}\kappa_{LL,ju}}{1+\kappa_{LL,ju}}}$, $\beta_{LL,ju} = \sqrt{\frac{\mu_{LL,ju}}{1+\kappa_{LL,ju}}}$, $\alpha_{R,u} = \sqrt{\frac{\mu_{R,u}\kappa_{R,u}}{1+\kappa_{R,u}}}$, $\beta_{R,u} = \sqrt{\frac{\mu_{R,u}}{1+\kappa_{R,u}}}$, $\alpha_{LR,ju} = \sqrt{\frac{\mu_{LR,ju}\kappa_{LR,ju}}{1+\kappa_{LR,ju}}}$, $\beta_{LR,ju} = \sqrt{\frac{\mu_{LR,ju}}{1+\kappa_{LR,ju}}}$, $\alpha_{LG,jk} = \sqrt{\frac{\mu_{LG,jk}\kappa_{LG,jk}}{1+\kappa_{LG,jk}}}$, $\beta_{LG,jk} = \sqrt{\frac{\mu_{LG,jk}}{1+\kappa_{LG,jk}}}$, $\alpha_{GL,u} = \sqrt{\frac{\mu_{GL,u}\kappa_{GL,u}}{1+\kappa_{GL,u}}}$, $\beta_{GL,u} = \sqrt{\frac{\mu_{GL,u}}{1+\kappa_{GL,u}}}$, $\alpha_{GR,u} = \sqrt{\frac{\mu_{GR,u}\kappa_{GR,u}}{1+\kappa_{GR,u}}}$, $\beta_{GR,u} = \sqrt{\frac{\mu_{GR,u}}{1+\kappa_{GR,u}}}$, $\bar{\boldsymbol{R}}_{LL,ju} = \bar{\boldsymbol{G}}_{LR,ju}\mathrm{diag}\left(\bar{\boldsymbol{h}}_{R,u}\right)$, and $\bar{\boldsymbol{r}}_{GL,ju} = \bar{\boldsymbol{g}}_{GR,u}\mathrm{diag}\left(\bar{\boldsymbol{h}}_{R,u}\right)$. In addition, $\boldsymbol{\Psi}_k$ in (9c) converted from (7) can be expressed as

$$\boldsymbol{\Psi}_{jk} = \beta_{LG,jk}\boldsymbol{I}_N + \alpha_{LG,jk}\bar{\boldsymbol{h}}_{LG,jk}\bar{\boldsymbol{h}}_{LG,jk}^H. \tag{12}$$

The constraint (9b) in (P2) remains a non-convex fractional expression. Using the quadratic transform [46], we convert this into a non-fractional form. This transform is effective for addressing fractional programming in our newly formulated optimization problem. Similar problems involving both max-min fairness and interference thresholds are relatively rare in existing RIS and SatCom literature. Specifically, by introduc-

$$\mathrm{SINR}_{\mathrm{u}}^{\mathrm{sCSI,AP,CF}}=\frac{\sum_{j\in\mathcal{J}}\boldsymbol{w}_{ju}^{H}\boldsymbol{\Theta}_{ju}\boldsymbol{w}_{ju}}{\sum_{j\in\mathcal{J}}\sum_{i\in\mathcal{U}}\boldsymbol{w}_{ji}^{H}\boldsymbol{\Xi}_{ju}\boldsymbol{w}_{ji}-\sum_{j\in\mathcal{J}}\boldsymbol{w}_{ju}^{H}\boldsymbol{\Theta}_{ju}\boldsymbol{w}_{ju}+f_1(\boldsymbol{\Phi}_u)+\sigma_u^2} \tag{10}$$

ing $U\times J$ complex-valued vectors $\{\boldsymbol{z}_{ju}, j\in\mathcal{J}, u\in\mathcal{U}\}$, $\mathrm{SINR}_{\mathrm{u}}^{\mathrm{sCSI,AP,CF}}$ in (9b) can be transformed into

$$\begin{aligned} f_2\left(\boldsymbol{W},\boldsymbol{\Phi}_u,\boldsymbol{z}_{ju}\right)=&\\ &\sum_{j\in\mathcal{J}}2\mathrm{Re}\{\boldsymbol{z}_{ju}^{H}\boldsymbol{\Theta}_{ju}^{\mathrm{CH}}\boldsymbol{w}_{ju}\}-\boldsymbol{z}_{ju}^{H}(f_1(\boldsymbol{\Phi}_u)+\sigma_u^2\\ &+\sum_{j\in\mathcal{J}}\sum_{i\in\mathcal{U}}\boldsymbol{w}_{ji}^{H}\boldsymbol{\Xi}_{ju}\boldsymbol{w}_{ji}-\sum_{j\in\mathcal{J}}\boldsymbol{w}_{ju}^{H}\boldsymbol{\Theta}_{ju}\boldsymbol{w}_{ju})\boldsymbol{z}_{ju}, \end{aligned} \tag{13}$$

where $\boldsymbol{\Theta}_{ju}^{\mathrm{CH}}$ is an upper triangular matrix obtained by Cholesky decomposition from $\boldsymbol{\Theta}_{ju}$, i.e., $\boldsymbol{\Theta}_{ju}=(\boldsymbol{\Theta}_{ju}^{\mathrm{CH}})^{H}\boldsymbol{\Theta}_{ju}^{\mathrm{CH}}$.

After quadratic transformation, there are three subproblems called 1) quadratic parameters updating, 2) satellite precoding, and 3) RIS passive beamforming to be solved alternatingly. Specifically, quadratic parameters can be updated as follows

$$\boldsymbol{z}_{ju}^{*}=\frac{\boldsymbol{\Theta}_{ju}^{\mathrm{CH}}\boldsymbol{w}_{ju}}{\sum_{j\in\mathcal{J}}\sum_{i\in\mathcal{U}}\boldsymbol{w}_{ji}^{H}\boldsymbol{\Xi}_{ju}\boldsymbol{w}_{ji}-\sum_{j\in\mathcal{J}}\boldsymbol{w}_{ju}^{H}\boldsymbol{\Theta}_{ju}\boldsymbol{w}_{ju}+f_1\left(\boldsymbol{\Phi}_u\right)+\sigma_u^2}. \tag{14}$$

Then, we can substitute (13) into (9b) and further introduce a set of U real-valued variables $\boldsymbol{\lambda}=[\lambda_1,\cdots,\lambda_U]$ to rewritten (9b) in a convex form, as shown in constraints (15b) and (15c) in the following equivalent optimization problem (P3).

$$(\mathrm{P3}):\max_{\boldsymbol{W},\gamma,\boldsymbol{\lambda}}\ \gamma \tag{15a}$$

$$\mathrm{s.t.}\sum_{j\in\mathcal{J}}2\mathrm{Re}\{\boldsymbol{z}_{ju}^{H}\boldsymbol{\Theta}_{ju}^{\mathrm{CH}}\boldsymbol{w}_{ju}\}-\boldsymbol{z}_{uj}^{H}\lambda_u\boldsymbol{z}_{uj}\geq\gamma,\forall u\in\mathcal{U}, \tag{15b}$$

$$f_1(\boldsymbol{\Phi}_u)+\sigma_u^2+\sum_{j\in\mathcal{J}}\sum_{i\in\mathcal{U}}\boldsymbol{w}_{ji}^{H}\boldsymbol{\Xi}_{ju}\boldsymbol{w}_{ji}-\sum_{j\in\mathcal{J}}\boldsymbol{w}_{ju}^{H}\boldsymbol{\Theta}_{ju}\boldsymbol{w}_{ju}\leq\lambda_u,\forall u\in\mathcal{U}, \tag{15c}$$

(8b), (9c).

(P3) is a standard convex problem that can be efficiently solved by existing methods or convex optimization tools [47].

B. RIS Passive Beamforming

As for the RIS passive beamforming optimization subproblem with given $\{\boldsymbol{z}_{uj}\}$ and $\boldsymbol{W}$, we can recast the subproblem for each RIS in a distributed manner as follows

$$(\mathrm{P4.u}):\max_{\{\boldsymbol{\phi}_u\}_{u=1}^{U}}\frac{f_4\left(\boldsymbol{\phi}_u\right)}{f_1(\boldsymbol{\phi}_u)+\sum_{i\in\mathcal{U}}f_3\left(\boldsymbol{\phi}_i\right)-f_4(\boldsymbol{\phi}_u)+\sigma_u^2} \tag{16a}$$

$$\mathrm{s.t.}f_4(\boldsymbol{\phi}_u)=\sum_{j\in\mathcal{J}}\boldsymbol{\phi}_u\boldsymbol{C}_{ju}\boldsymbol{\phi}_u^{H}+2\mathrm{Re}\left\{\boldsymbol{\phi}_u\boldsymbol{c}_{ju}\right\}+c_{4,ju} \tag{16b}$$

$$f_3\left(\boldsymbol{\phi}_u\right)=\sum_{j\in\mathcal{J}}\boldsymbol{\phi}_u\boldsymbol{C}_{ju}\boldsymbol{\phi}_u^{H}+2\mathrm{Re}\left\{\boldsymbol{\phi}_u\boldsymbol{c}_{ju}\right\}+c_{3,ju} \tag{16c}$$

$$f_1(\boldsymbol{\phi}_u)=\sum_{j\in\mathcal{J}}\boldsymbol{\phi}_u\boldsymbol{B}_u\boldsymbol{\phi}_u^{H}+2\mathrm{Re}\left\{\boldsymbol{\phi}_u\boldsymbol{b}_u\right\}+b_u \tag{16d}$$

$$|\phi_{u,m}|^2=1,\forall u\in\mathcal{U},\forall m, \tag{16e}$$

where $\boldsymbol{C}_{ju}$, $\boldsymbol{c}_{ju}$, $c_{3,ju}$, and $c_{4,ju}$ in (16b) and (16c) are derived from (11a) and (11b) with fixed $\boldsymbol{W}$ given as follows

$$\begin{aligned}\boldsymbol{C}_{ju}=&\alpha_{LR,ju}^2\alpha_{R,u}^2\mathrm{diag}(\bar{\boldsymbol{h}}_{R,u}^{H})\bar{\boldsymbol{G}}_{LR,ju}^{H}\boldsymbol{w}_{ju}\\ &\cdot\boldsymbol{w}_{ju}^{H}\bar{\boldsymbol{G}}_{LR,ju}\mathrm{diag}(\bar{\boldsymbol{h}}_{R,u}),\end{aligned} \tag{17a}$$

$$\boldsymbol{c}_{ju}=\alpha_{LL,ju}\alpha_{R,u}\alpha_{LR,ju}\mathrm{diag}(\bar{\boldsymbol{h}}_{R,u}^{H})\bar{\boldsymbol{G}}_{LR,ju}^{H}\boldsymbol{w}_{ju}\boldsymbol{w}_{ju}^{H}\bar{\boldsymbol{h}}_{LL,ju}, \tag{17b}$$

$$c_{4,ju}=\alpha_{LL,ju}^2\boldsymbol{w}_{ju}^{H}\bar{\boldsymbol{h}}_{LL,ju}\bar{\boldsymbol{h}}_{LL,ju}^{H}\boldsymbol{w}_{ju}, \tag{17c}$$

$$\begin{aligned}c_{3,ju}=&c_{4,ju}+\alpha_{LR,ju}^2\beta_{R,u}^2\boldsymbol{w}_{ju}^{H}\bar{\boldsymbol{G}}_{LR,ju}\bar{\boldsymbol{G}}_{LR,ju}^{H}\boldsymbol{w}_{ju}\\ &+\left(\beta_{LL,ju}^2+\beta_{LR,ju}^2\mu_{R,u}M\right)\boldsymbol{w}_{ju}^{H}\boldsymbol{w}_{ju},\end{aligned} \tag{17d}$$

and $\boldsymbol{B}_u$, $\boldsymbol{b}_u$, and b_u in (16d) are derived from (11c) as follows

$$\boldsymbol{B}_u=\alpha_{GR,ju}^2\alpha_{R,u}^2\mathrm{diag}(\bar{\boldsymbol{h}}_{R,u}^{H})\bar{\boldsymbol{g}}_{GR,u}^{\dagger}\bar{\boldsymbol{g}}_{GR,u}^{T}\mathrm{diag}(\bar{\boldsymbol{h}}_{R,u}), \tag{18a}$$

$$\boldsymbol{b}_u=\alpha_{GL,u}\alpha_{R,u}\alpha_{GR,u}\mathrm{diag}(\bar{\boldsymbol{h}}_{R,u}^{H})\bar{\boldsymbol{g}}_{GR,u}^{H}\bar{h}_{GL,u}, \tag{18b}$$

$$b_u=\alpha_{GL,u}^2+\alpha_{GR,u}^2\beta_{R,u}^2M+\beta_{GL,u}^2+\beta_{GR,u}^2\mu_{R,u}M. \tag{18c}$$

Given the unit-modulus constraint (16e), we apply a manifold optimization technique to derive an optimal solution for (P4.u). Specifically, (16e) defines a complex sphere manifold [48] in a Euclidean space, which can be denoted by

$$\mathcal{M}=\{\boldsymbol{\phi}_u\in\mathbb{C}^M\mid[\boldsymbol{\phi}_u^{H}\boldsymbol{\phi}_u]_{m,m}=1,\forall m=1,\ldots,M\}. \tag{19}$$

The tangent space of the complex sphere manifold $\mathcal{M}$ at the point $\boldsymbol{\phi}_u^{(l)}$ is defined as the space that contains all tangent vectors of $\mathcal{M}$ at $\boldsymbol{\phi}_u^{(l)}$, and denoted by $T_{\boldsymbol{\phi}_u^{(l)}}\mathcal{M}$ as follows

$$T_{\boldsymbol{\phi}_u^{(l)}}\mathcal{M}=\{\boldsymbol{t}\in\mathbb{C}^M\mid[\boldsymbol{t}(\boldsymbol{\phi}_u^{(l)})^{H}]_{m,m}=0,\forall m=1,\ldots,M\}, \tag{20}$$

where l denotes the iteration number. The Riemannian gradient is a vector field on the manifold $\mathcal{M}$, given by the projection of Euclidean gradient on the tangent space $T_{\boldsymbol{\phi}^{(l)}}\mathcal{M}$ as follows

$$\begin{aligned}\mathrm{Rgrad}_{\boldsymbol{\phi}_u^{(l)}}F_{AP}(\boldsymbol{\phi}_u^{(l)})=&\nabla F_{AP}(\boldsymbol{\phi}_u^{(l)})\\ &-\mathrm{Re}\left\{\nabla F_{AP}(\boldsymbol{\phi}_u^{(l)})\odot(\boldsymbol{\phi}_u^{(l)})^{\dagger}\right\}\odot\boldsymbol{\phi}_u^{(l)},\end{aligned} \tag{21}$$

where $\odot$ represents the Hadamard product operator, $F_{AP}(\boldsymbol{\phi}_u^{(l)})$ denotes effective SINR (16a) for u-th LU aided by its RIS, and $\nabla F_{AP}(\boldsymbol{\phi}_u^{(l)})$ denotes the corresponding Euclidean gradient, which can be respectively written as

$$\begin{aligned}\nabla F_{AP}(\boldsymbol{\phi}_u)=&(f_1(\boldsymbol{\phi}_u)+\sum_{i\in\mathcal{U}}f_3(\boldsymbol{\phi}_i)-f_4(\boldsymbol{\phi}_u)+\sigma_u^2)^{-2}\\ &\times\big(\nabla f_4(\boldsymbol{\phi}_u)(f_1(\boldsymbol{\phi}_u)+\sum_{i\in\mathcal{U}}f_3(\boldsymbol{\phi}_i)-f_4(\boldsymbol{\phi}_u)+\sigma_u^2)\\ &-f_4(\boldsymbol{\phi}_u)(\nabla f_1(\boldsymbol{\phi}_u)+\sum_{i\in\mathcal{U}}\nabla f_3\left(\boldsymbol{\phi}_i\right)-\nabla f_4(\boldsymbol{\phi}_u))\big),\end{aligned} \tag{22a}$$

$$\nabla f_4(\boldsymbol{\phi}_u)\triangleq\nabla f_3(\boldsymbol{\phi}_u)=\sum_{j\in\mathcal{J}}2\boldsymbol{C}_{ju}\boldsymbol{\phi}_u+2\boldsymbol{c}_{ju}^{H}, \tag{22b}$$

$$\nabla f_1(\boldsymbol{\phi}_u)=2\boldsymbol{B}_u\boldsymbol{\phi}_u+2\boldsymbol{b}_u^{H}. \tag{22c}$$

Algorithm 1 Alternating Optimization Algorithm for (P2).

1: Initialize the satellite precoding matrix $\boldsymbol{W} = \boldsymbol{W}^{(0)}$ by first generating an arbitrary feasible solution satisfying (7) and (8b) and then optimizing $\boldsymbol{W}$ by (P3) without RISs.
2: **repeat**
3: Update quadratic transform parameters $\{\boldsymbol{z}_{ju}\}$ via (14).
4: Solve problem (P3) via convex optimization methods or CVX and obtain an optimal solution $\boldsymbol{W}^{l_1+1}$.
5: Solve problem (P4.u) for each RIS via manifold optimization and obtain U optimal solutions $\{\boldsymbol{\phi}_u^{l+1}\}_{u=1}^U$.
6: Update $l_1 = l_1 + 1$.
7: **until** The fractional increase of γ is below a threshold $\epsilon > 0$ or the maximum number of iterations $L_{1,\max}$ is reached.

Finally, the Riemannian gradient descent (RGD) or Riemannian conjugate gradient (RCG) method [48] can be implemented to solve (P4.u). Taking RGD as an example, the descent direction ξ^l at the l-th iteration is determined by the negative counterpart of the Riemannian gradient as $\xi^l = -\mathrm{Rgrad}_{\boldsymbol{\phi}_u^{(l)}} F_{AP}(\boldsymbol{\phi}_u^{(l)})$, and then RIS phase shifts $\boldsymbol{\phi}_u^{(l+1)}$ at l+1-th iteration is updated as $\boldsymbol{\phi}_u^{(l+1)} = \left[\frac{(\boldsymbol{\phi}_u^{(l)}+\alpha^l\xi^l)_m}{|(\boldsymbol{\phi}_u^{(l)}+\alpha^l\xi^l)_m|}\right]$, where α^l is the step size.

C. Overall Algorithm and Its Discussion

The overall AO-based algorithm design is detailed in Algorithm 1, deriving a solution for the original problem (P1) by alternately solving (P3) and (P4.u) in an iterative manner. The algorithm guarantees convergence with local optimality because the minimum SINR value is non-decreased in each subproblem and iteration. The overall computational complexity of Algorithm 1 is $\mathcal{O}(L_1L_2(JU^2NM^2)+L_1(JN)^{3.5})$, where L_1 is the overall number of AO iterations, the complexity of solving (P3) is $\mathcal{O}((JN)^{3.5})$ by the interior-point method and the complexity of solving (P4.u) is $\mathcal{O}(L_2(JU^2NM^2)$ mainly originated from cost and gradient calculations with L_2 denoting iteration times in manifold optimization.

While we clarify the reasonablity to asuume the GEO and LEO terminal are equipped with single antenna, it is more pratical to consider user terminal are equpped with multiple antenna, especially for LEO terminal to improve communication performance. However, our focus on the RIS-aided multi-satellite transmission scheme distinguishes our work, presenting unique challenges in deriving closed-form expressions and algorithm design that cannot be directly addressed by existing methods. Additionally, our proposed scheme can be extended to multi-antenna terminals with single data stream transmission between a LEO satellite and a LU. In the adaptive precoding case, the modified objective function will only add summation terms represented for the divesity gain at receiver to (14), (17), and (18), and thus the proposed AO-based algorithm can continue to use.

IV. Cooperative Beamforming Design Under MR Precoding with Adaptive-Precoding Results

In the adaptive precoding case depicted earlier, after optimizing cooperative beamforming, the processing satellite must share the phase shift matrices with the RISs and precoding matrices with the other cooperative satellites. Employing MR precoding can reduce the signaling overhead in the satellite network through conjugate beamforming [23]. In this setup, only the power allocation information needs to be exchanged between satellites, which reduces signaling overhead by $\frac{1}{N}$. More importantly, another significant benefit of MR precoding is its ability to leverage two-timescale CSI effectively, which will be elaborated on in Section VI.

In this section, we reformulate the original problem (P1) by incorporating MR precoding, from which we further derive closed-form expressions. Then, we propose a cooperative beamforming design that leverages the results obtained from the previous adaptive precoding case. Recall that the MR precoding under perfect instantaneous CSI is written as

$$\boldsymbol{w}_{ju}^{\mathrm{iCSI}} = \sqrt{p_{ju}}(\boldsymbol{h}_{LL,ju} + \boldsymbol{G}_{LR,ju}\boldsymbol{\Phi}_u\boldsymbol{h}_{R,u}), \tag{23}$$

where p_{ju} denotes the power allocation parameter to guarantee total beam power constraint. However, exploiting only statistical CSI, the MR precoding vector can be expressed as

$$\boldsymbol{w}_{ju}^{\mathrm{sCSI}} \triangleq \sqrt{p_{ju}}\mathbb{E}\left\{\boldsymbol{h}_{LL,ju} + \boldsymbol{G}_{LR,ju}\boldsymbol{\Phi}_u\boldsymbol{h}_{R,u}\right\}, \tag{24a}$$

$$= \sqrt{p_{ju}}\big(\bar{\boldsymbol{h}}_{LL,ju} + \bar{\boldsymbol{G}}_{LR,ju}\boldsymbol{\Phi}_u\bar{\boldsymbol{h}}_{R,u}\big). \tag{24b}$$

i.e., the LoS part of the superimposed channel vectors.

A. Closed-Form Optimization Problem Under MR Precoding

With MR precoding at the satellite, the cooperative beamforming design is converted into a joint power allocation and RIS phase shift optimization problem rewritten as follows

$$(\mathrm{P5}): \max_{\{\boldsymbol{\Phi}_u\}_{u=1}^U, \boldsymbol{p}} \min_{\forall u\in\mathcal{U}} \left\{\mathrm{SINR}_u^{\mathrm{sCSI,MR}}\right\} \tag{25a}$$

$$\text{s.t.} \sum_{j\in\mathcal{J}}\sum_{u\in\mathcal{U}} p_{ju}\mathbb{E}\{|\boldsymbol{h}_{LG,jk}^H\mathbb{E}\left\{\boldsymbol{h}_{LL,ju} + \boldsymbol{G}_{LR,ju}\boldsymbol{\Phi}_u\boldsymbol{h}_{R,u}\right\}|^2\} \leq \varsigma_k, \forall k\in\mathcal{K}, \tag{25b}$$

$$\sum_{u\in\mathcal{U}} p_{ju}\left\|\mathbb{E}\{\boldsymbol{h}_{LL,ju}+\boldsymbol{h}_{R,u}\boldsymbol{\Phi}_u\boldsymbol{G}_{LR,ju}\}\right\|^2 \leq P_T, \forall j\in\mathcal{J}, \tag{25c}$$

$$|\phi_{u,m}|^2 = 1, \forall u\in\mathcal{U}, \forall m, \tag{25d}$$

where $\mathrm{SINR}_u^{\mathrm{sCSI,MR}}$ in (25a) is expressed in (26) at the top of the next page, and $\boldsymbol{h}_{L,ju} \triangleq \boldsymbol{h}_{LL,ju}+\boldsymbol{G}_{LR,ju}\boldsymbol{\Phi}_u\boldsymbol{h}_{R,u}$ denotes superimposed satellite-to-user channels for brevity. The implicit expression of RIS phase shifts involves expectation terms, making it intractable to handle and optimize. Thus, the primary focus is deriving the closed-form expression of (P5).

Accordingly, after calculation, we rewrite (P5) into (P6) as

$$(\mathrm{P6}): \max_{\{\boldsymbol{\Phi}_u\}_{u=1}^U, \boldsymbol{p}} \min_{\forall u\in\mathcal{U}} \mathrm{SINR}_u^{\mathrm{cCSI,MR,CF}}(\boldsymbol{\phi}_1,\ldots,\boldsymbol{\phi}_U) \tag{27a}$$

$$\text{s.t.} \sum_{j\in\mathcal{J}}\sum_{u\in\mathcal{U}} p_{ju}f_{7,juk}(\boldsymbol{\phi}_u) - \varsigma_k \leq 0, \forall k\in\mathcal{K}, \tag{27b}$$

$$\sum_{u\in\mathcal{U}} p_{ju}\sqrt{f_{5,ju}(\boldsymbol{\phi}_u)} - P_T \leq 0, \forall j\in\mathcal{J}, \tag{27c}$$

$$|\phi_{u,m}|^2 = 1, \forall u\in\mathcal{U}, \forall m, \tag{27d}$$

where $\mathrm{SINR}_u^{\mathrm{cCSI,MR,CF}}(\boldsymbol{\phi}_1,\ldots,\boldsymbol{\phi}_U)$ denotes the closed-form expression of LUs' SINR in (28) at the top of next page, and

$$\mathrm{SINR}_u^{\mathrm{sCSI,MR}} = \frac{\sum_{j\in\mathcal{J}} p_{ju}\left|\mathbb{E}\{\boldsymbol{h}_{L,ju}^H \mathbb{E}\{\boldsymbol{h}_{L,ju}\}\}\right|^2}{\sum_{j\in\mathcal{J}}\sum_{i\in\mathcal{U}} p_{ji}\mathbb{E}\{\left|\boldsymbol{h}_{L,ju}^H \mathbb{E}\left\{\boldsymbol{h}_{L,ji}\right\}\right|^2\} - \sum_{j\in\mathcal{J}} p_{ju}\left|\mathbb{E}\{\boldsymbol{h}_{L,ju}^H \mathbb{E}\left\{\boldsymbol{h}_{L,ju}\right\}\}\right|^2 + \mathbb{E}\{|h_{G,u}^H|^2\} + \sigma_u^2} \tag{26a}$$

$$= \sum_{j\in\mathcal{J}} p_{ju}\left|\left\|\mathbb{E}\left\{\boldsymbol{h}_{LL,ju} + \boldsymbol{G}_{LR,ju}\boldsymbol{\Phi}_u\boldsymbol{h}_{R,u}\right\}\right\|^2\right|^2 \cdot \left(\sum_{j\in\mathcal{J}}\sum_{i\in\mathcal{U}} p_{ji}\mathbb{E}\left\{\left|(\boldsymbol{h}_{LL,ju}^H + \boldsymbol{h}_{R,u}^H\boldsymbol{\Phi}_u^H\boldsymbol{G}_{LR,ju}^H)\bar{\boldsymbol{h}}_{L,ji}\right|^2\right\}\right.$$
$$\left. - \sum_{j\in\mathcal{J}} p_{ju}\left|\left\|\mathbb{E}\left\{\boldsymbol{h}_{LL,ju} + \boldsymbol{G}_{LR,ju}\boldsymbol{\Phi}_u\boldsymbol{h}_{R,u}\right\}\right\|^2\right|^2 + \mathbb{E}\left\{\left|h_{GL,u}^H + \boldsymbol{h}_{R,u}^H\boldsymbol{\Phi}_u\boldsymbol{g}_{GR,u}^\dagger\right|^2\right\} + \sigma_u^2\right)^{-1} \tag{26b}$$

$$\mathrm{SINR}_u^{\mathrm{cCSI,MR,CF}}\left(\boldsymbol{\phi}_1,\ldots,\boldsymbol{\phi}_U\right) = \frac{\sum_{j\in\mathcal{J}} p_{ju} f_{5,ju}(\boldsymbol{\phi}_u)}{\sum_{j\in\mathcal{J}}\sum_{i\in\mathcal{U}} p_{ji} f_{6,jui}(\boldsymbol{\phi}_u,\boldsymbol{\phi}_i) - \sum_{j\in\mathcal{J}} p_{ju} f_{5,ju}(\boldsymbol{\phi}_u) + f_4(\boldsymbol{\phi}_u) + \sigma_u^2} \tag{28}$$

$$\begin{aligned}
&f_{6,jui}(\boldsymbol{\phi}_u,\boldsymbol{\phi}_i) = \\
&2\chi_{1,ju}\alpha_{LL,ji}^2 \mathrm{Re}\{\bar{\boldsymbol{h}}_{LL,ju}^H \bar{\boldsymbol{h}}_{LL,ji} \bar{\boldsymbol{h}}_{LL,ji}^H \bar{\boldsymbol{R}}_{LL,ju}\boldsymbol{\phi}_u\} + \alpha_{LL,ji}^2 \\
&\times\chi_{2,ju}|\bar{\boldsymbol{h}}_{LL,ji}^H \bar{\boldsymbol{R}}_{LL,ju}\boldsymbol{\phi}_u|^2 + \alpha_{LL,ju}^2\chi_{1,ji} 2\mathrm{Re}\{\boldsymbol{h}_{LL,ji}^H \bar{\boldsymbol{h}}_{LL,ju} \\
&\times\bar{\boldsymbol{h}}_{LL,ju}^H \bar{\boldsymbol{R}}_{LL,ji}\boldsymbol{\phi}_i\} + \chi_{4,ju}\chi_{1,ji} 2\mathrm{Re}\{\boldsymbol{h}_{LL,ji}^H \bar{\boldsymbol{G}}_{LR,ju} \bar{\boldsymbol{G}}_{LR,ju}^H \\
&\times\bar{\boldsymbol{R}}_{LL,ji}\boldsymbol{\phi}_i\} + \chi_{3,ju}\chi_{1,ji} 2\mathrm{Re}\{\boldsymbol{h}_{LL,ji}^H \bar{\boldsymbol{R}}_{LL,ji}\boldsymbol{\phi}_i\} + \chi_{4,ju}\chi_{2,ji} \\
&\times|\boldsymbol{\phi}_i^H \bar{\boldsymbol{R}}_{LL,ji}^H \bar{\boldsymbol{G}}_{LR,ju}|^2 + \alpha_{LL,ju}^2\chi_{2,ji}|\boldsymbol{\phi}_i^H \bar{\boldsymbol{R}}_{LL,ji}^H \bar{\boldsymbol{h}}_{LL,ju}|^2 \\
&+\chi_{3,ju}\chi_{2,ji}\left\|\bar{\boldsymbol{R}}_{LL,ji}\boldsymbol{\phi}_i\right\|^2 + \chi_{2,ju}\chi_{2,ji}|\boldsymbol{\phi}_i^H \bar{\boldsymbol{R}}_{LL,ji}^H \bar{\boldsymbol{R}}_{LL,ju}\boldsymbol{\phi}_u|^2 \\
&+ 2\chi_{1,ju}\chi_{1,ji}\mathrm{Re}\{\bar{\boldsymbol{h}}_{LL,ji}^H \bar{\boldsymbol{R}}_{LL,ju}\boldsymbol{\phi}_u \cdot \bar{\boldsymbol{h}}_{LL,ju}^H \bar{\boldsymbol{R}}_{LL,ji}\boldsymbol{\phi}_i\} \\
&+ 2\chi_{1,ju}\chi_{1,ji}\mathrm{Re}\{\bar{\boldsymbol{h}}_{LL,ji}^H \bar{\boldsymbol{h}}_{LL,ju}\boldsymbol{\phi}_u^H \bar{\boldsymbol{R}}_{LL,ju}^H \bar{\boldsymbol{R}}_{LL,ji}\boldsymbol{\phi}_i\} \\
&+ 2\chi_{1,ju}\chi_{2,ji}\mathrm{Re}\{\boldsymbol{\phi}_i^H \bar{\boldsymbol{R}}_{LL,ji}^H \bar{\boldsymbol{R}}_{LL,ju}\boldsymbol{\phi}_u \cdot \bar{\boldsymbol{h}}_{LL,ju}^H \bar{\boldsymbol{R}}_{LL,ji}\boldsymbol{\phi}_i\} \\
&+ 2\chi_{2,ju}\chi_{1,ji}\mathrm{Re}\{\boldsymbol{h}_{LL,ji}^H \bar{\boldsymbol{R}}_{LL,ju}\boldsymbol{\phi}_u \cdot \boldsymbol{\phi}_u^H \bar{\boldsymbol{R}}_{LL,ju}^H \bar{\boldsymbol{R}}_{LL,ji}\boldsymbol{\phi}_i\} \\
&+ \chi_{3,ju}\alpha_{LL,ji}^2 N + \alpha_{LL,ju}^2 a_{LL,ji}^2 |\boldsymbol{h}_{LL,ji}^H \bar{\boldsymbol{h}}_{LL,ju}|^2 \\
&+ \chi_{4,ju}\alpha_{LL,ji}^2 |\boldsymbol{h}_{LL,ji}^H \bar{\boldsymbol{G}}_{LR,ju}|^2,
\end{aligned} \tag{29a}$$

$$f_{5,ju}(\boldsymbol{\phi}_u) = \left\|\alpha_{LL,ju}\bar{\boldsymbol{h}}_{LL,ju} + \alpha_{LR,ju}\alpha_{R,u}\bar{\boldsymbol{R}}_{LL,ju}\boldsymbol{\phi}_u\right\|^4, \tag{29b}$$

$$\begin{aligned}
&f_{7,juk}(\boldsymbol{\phi}_u) = \\
&\alpha_{LG,jk}^2|\alpha_{LL,ju}\bar{\boldsymbol{h}}_{LG,jk}^H \bar{\boldsymbol{h}}_{LL,ju} + \alpha_{LR,ju}\alpha_{R,u}\bar{\boldsymbol{h}}_{LG,jk}^H \bar{\boldsymbol{R}}_{LL,ju}\boldsymbol{\phi}_u|^2 \\
&\quad + \beta_{LG,jk}^2\|\alpha_{LL,ju}\bar{\boldsymbol{h}}_{LL,ju} + \alpha_{LR,ju}\alpha_{R,u}\bar{\boldsymbol{R}}_{LL,ju}\boldsymbol{\phi}_u\|^2,
\end{aligned} \tag{29c}$$

where we further denote $\chi_{1,ju}=\alpha_{LL,ju}\alpha_{R,u}\alpha_{LR,ju}$, $\chi_{2,ju}=\alpha_{R,u}^2\alpha_{LR,ju}^2$, $\chi_{3,ju}=(\beta_{LL,ju}^2+\beta_{LR,ju}^2\mu_{R,u}M)$, and $\chi_{4,ju}=\alpha_{LR,ju}^2\beta_{R,u}^2$ for brevity.

B. Power Allocation with RIS Phase Shifts Results Under Adaptive Precoding Configuration

Intuitively, the reformulated closed-form optimization problem (P6) can be decoupled into two subproblems: RIS phase shifts design and power allocation, while the detailed procedures are left in the next section. Here, we focus on an effective design that utilizes RIS phase shifts optimized through Algorithm 1 under adaptive precoding. Then, given RIS phase shifts, we only need to optimize power allocation at satellites via fractional programming. Similar to (13)-(15) in Section III-A, the power allocation problem is written as

Algorithm 2 Power Allocation with Given $\boldsymbol{\Phi}$ for (P6).

1: Substituting the RIS phase shifts $\boldsymbol{\Phi} = \boldsymbol{\Phi}^{\mathrm{A1}}$ optimized by Algorithm 1 into closed-from (P6) and set $l_3 = 0$.
2: **repeat**
3: Update quadratic transform parameters $\boldsymbol{y}^{(l_3+1)}$ via (32).
4: Solve problem (P7), obtain an optimal solution $\boldsymbol{p}^{(l_3+1)}$.
5: Update $l_3 = l_3 + 1$.
6: **until** Convergence.

$$\begin{aligned}
(\mathrm{P7}):\max_{\boldsymbol{P},\gamma}\ & \gamma && (30a)\\
\text{s.t.}\ & \sum_{j\in\mathcal{J}} 2y_{ju}\sqrt{p_{ju}s_{1,ju}} - y_{ju}^2\Big(\sum_{j\in\mathcal{J}}\sum_{i\in\mathcal{U},} p_{ji}s_{2,jui} \\
& \qquad - \sum_{j\in\mathcal{J}} p_{ju}s_{1,ju} + s_{3,u} + \sigma_u^2\Big) > \gamma && (30b)\\
& \sum_{j\in\mathcal{J}}\sum_{u\in\mathcal{U}} p_{ju}s_{4,juk} \le \varsigma_k, \forall k\in\mathcal{K}, && (30c)\\
& \sum_{u\in\mathcal{U}} p_{ju}s_{2,juu} \le P_T, \forall j\in\mathcal{J}, && (30d)
\end{aligned}$$

where we introduce $U\times J$ auxiliary variables $\{y_{ju}, j\in\mathcal{J}, u\in\mathcal{U}\}$ for quadratic transform and $s_{1,ju}, s_{2,jui}, s_{3,u}$, and $s_{4,juk}$ denote the effective superimposed channel gains with given RIS phase shifts as below

$$s_{1,ju} \triangleq \left|\mathbb{E}\{\boldsymbol{h}_{L,ju}^H \mathbb{E}\left\{\boldsymbol{h}_{L,ju}\right\}\}\right|^2 = f_{5,ju}(\boldsymbol{\phi}_u), \tag{31a}$$

$$s_{2,jui} \triangleq \mathbb{E}\{\left|\boldsymbol{h}_{L,ju}^H \mathbb{E}\left\{\boldsymbol{h}_{L,ji}\right\}\right|^2\} = f_{6,jui}(\boldsymbol{\phi}_u,\boldsymbol{\phi}_i), \tag{31b}$$

$$s_{3,u} \triangleq \mathbb{E}\{\left|h_{G,u}^H\right|^2\} = f_4(\boldsymbol{\phi}_u), \tag{31c}$$

$$s_{4,juk} \triangleq \mathbb{E}\{\left|\boldsymbol{h}_{LG,jk}^H \mathbb{E}\left\{\boldsymbol{h}_{L,ju}\right\}\right\} = f_{7,juk}(\boldsymbol{\phi}_u). \tag{31d}$$

Then, the quadratic parameters y_{ju} in (30b) are updated by

$$y_{ju}^* = \frac{\sqrt{p_{ju}s_{ju}}}{\sum_{j\in\mathcal{J}}\sum_{i\in\mathcal{U}} p_{ji}s_{2,jiu} - \sum_{j=1}^{J} p_{ju}s_{1,ju} + s_{3,u} + \sigma_u^2}. \tag{32}$$

C. Overall algorithm and computational complexity analysis

The details of the power allocation algorithm with given $\boldsymbol{\Phi}$ are summarized in Algorithm 2. Specifically, we substitute

the RIS phase shifts under adaptive precoding optimized by Algorithm 1 into the closed-form optimization problem (P6). Then, we can solve the power allocation subproblem (P7) via a fractional programming method, i.e., quadratic transform, similar to the process in (13)-(15). Besides the complexity brought by Algorithm 1, the main complexity of Algorithm 2 is $\mathcal{O}(L_3(JU)^{3.5})$ originating from solving the problem (P7).

V. Two-Stage Cooperative Beamforming Design under MR Precoding

In this section, we design cooperative beamforming with MR Precoding that does not rely on the RIS phase shifts outcome from Algorithm 1. We divide (P6) into subproblems for RIS phase shift design and power allocation, proposing a two-stage algorithm. Our emphasis is on designing RIS phase shifts, as the power allocation is addressed by Algorithm 2.

A. ES-SP-RMO Algorithm for RIS Phase Shifts Design

For the RIS phase shifts design subproblem with fixed power allocation parameters, we develop an exponential smoothing and sum-square penalty-assisted Riemannian manifold optimization-based (ES-SP-RMO) iterative algorithm. Specifically, the corresponding problem can be formulated as follows

$$\begin{aligned}(\text{P8}):\max_{\{\boldsymbol{\Phi}_u\}_{u=1}^U,\mu}\ & -\mu\log\sum_{u\in\mathcal{U}}\exp\left(-\text{SINR}_u^{\text{sCSI,MR,CF}}\left(\boldsymbol{\Phi}\right)/\mu\right)\\ &-\sum_{k\in\mathcal{K}}\Big(\sum_{j\in\mathcal{J}}\sum_{u\in\mathcal{U}}p_{ju}\mathbb{E}\{|\boldsymbol{h}_{LG,jk}^H\mathbb{E}\{\boldsymbol{h}_{L,ju}\}|^2-\varsigma_k\Big)^2 \quad (33a)\\ \text{s.t. }\ & |\phi_{u,m}|^2=1,\forall u\in\mathcal{U},\forall m, \quad (33b)\end{aligned}$$

where the second term in the objective function (33a) of (P8) is a sum-square penalty term [49] corresponding to constraint (52) to suppress LEO-GEO interference value, and the first term is a smoothed surrogate function for (27a) of (P6) with an introduced exponential smoothing parameter $\mu\geq 0$ [50],[51].

After exponential smoothing, the first term of (33a) satisfies

$$\begin{aligned}&-\mu\log\sum_{u\in\mathcal{U}}\exp\left(-\text{SINR}_u^{\text{sCSI,MR,CF}}\left(\boldsymbol{\Phi}\right)/\mu\right)\\ &\leq\min_{\forall u\in\mathcal{U}}\left\{\text{SINR}_u^{\text{sCSI,MR,CF}}\left(\boldsymbol{\Phi}\right)\right\}\\ &\leq-\mu\log\sum_{u\in\mathcal{U}}\exp\left(-\text{SINR}_u^{\text{sCSI,MR,CF}}\left(\boldsymbol{\Phi}\right)/\mu\right)+\mu\log U. \quad (34)\end{aligned}$$

Note that when μ is sufficiently small, the inequality (34) approaches equality, and the surrogate function leads to high approximation accuracy to the minimum SINR (27a). However, when μ is small, (P8) is nearly ill-conditioned and difficult to solve. Therefore, we can use an iterative strategy that solves a sequence of gradually more accurate approximations later.

With a fixed μ and power allocation, the RIS phase shift optimization problem can be written into (P9)

$$(\text{P9})\qquad \boldsymbol{\Phi}^*=\underset{|\phi_{u,m}|=1,\forall u,\forall m}{\arg\max}\quad F_{MR}\left(\boldsymbol{\Phi}\right) \quad (35)$$

where $F_{MR}\left(\boldsymbol{\Phi}\right)$ is a scalar-valued function of a manifold optimization problem with complex matrix variables as below

$$\begin{aligned}F_{MR}\left(\boldsymbol{\Phi}\right)=&-\mu\log\sum_{u\in\mathcal{U}}\exp\left(-\text{SINR}_u^{\text{cCSI,MR,CF}}\left(\boldsymbol{\Phi}\right)/\mu\right)\\ &-\sum_{k\in\mathcal{K}}\Big(\sum_{j\in\mathcal{J}}\sum_{u\in\mathcal{U}}p_{ju}f_{7,juk}\left(\boldsymbol{\phi}_u\right)-\varsigma_k\Big)^2. \quad (36)\end{aligned}$$

The corresponding Euclidean gradient of $F_{MR}\left(\boldsymbol{\Phi}\right)$ is a $U\times M$ complex matrix written as (37), where the Euclidean gradient of closed-form SINR expression is written in (38) at the top of next page, and partial derivatives $\frac{\partial f_{5,ju}(\boldsymbol{\phi}_u)}{\partial\boldsymbol{\phi}_u}$, $\frac{\partial f_{6,jui}(\boldsymbol{\phi}_u,\boldsymbol{\phi}_i)}{\partial\boldsymbol{\phi}_u}$ and $\frac{\partial f_{6,jui}(\boldsymbol{\phi}_u,\boldsymbol{\phi}_i)}{\partial\boldsymbol{\phi}_i}$ with $i\neq u$, $\frac{\partial f_{6,juu}(\boldsymbol{\phi}_u)}{\partial\boldsymbol{\phi}_u}$, and $\frac{\partial f_{7,juk}(\boldsymbol{\phi}_u)}{\partial\boldsymbol{\phi}_u}$ can be written in (39a)-(39e), respectively, as below

$$\begin{aligned}\frac{\partial f_{5,ju}(\boldsymbol{\phi}_u)}{\partial\boldsymbol{\phi}_u}=&\,4\|\alpha_{LL,ju}\bar{\boldsymbol{h}}_{LL,ju}+\alpha_{LR,ju}\alpha_{R,u}\bar{\boldsymbol{R}}_{LL,ju}\boldsymbol{\phi}_u\|^2\\ &\cdot(\chi_{1,ju}\bar{\boldsymbol{R}}_{LL,ju}^H\bar{\boldsymbol{h}}_{LL,ju}+\chi_{2,ju}\bar{\boldsymbol{R}}_{LL,ju}^H\bar{\boldsymbol{R}}_{LL,ju}\boldsymbol{\phi}_u), \quad (39a)\\ \frac{\partial f_{6,jui}(\boldsymbol{\phi}_u,\boldsymbol{\phi}_i)}{\partial\boldsymbol{\phi}_u}=&\,\bar{\boldsymbol{R}}_{LL,ju}^H\big(4\chi_{1,ji}\text{Re}\{\boldsymbol{h}_{LL,ji}\boldsymbol{\phi}_i^H\bar{\boldsymbol{R}}_{LL,ji}^H\}\\ &+2\chi_{2,ji}\bar{\boldsymbol{R}}_{LL,ji}\boldsymbol{\phi}_i\boldsymbol{\phi}_i^H\bar{\boldsymbol{R}}_{LL,ji}^H+2a_{LL,ji}^2\bar{\boldsymbol{h}}_{LL,ji}\bar{\boldsymbol{h}}_{LL,ji}^H\big)\\ &\times\big(\chi_{1,ju}\bar{\boldsymbol{h}}_{LL,ju}+\chi_{2,ju}\bar{\boldsymbol{R}}_{LL,ju}\boldsymbol{\phi}_u\big) \quad (39b)\\ \frac{\partial f_{6,jui}(\boldsymbol{\phi}_u,\boldsymbol{\phi}_i)}{\partial\boldsymbol{\phi}_i}=&\,\frac{\partial f_{6,jui}(\boldsymbol{\phi}_u,\boldsymbol{\phi}_i)}{\partial\boldsymbol{\phi}_u}\Big|_{i\leftrightarrow u}+\bar{\boldsymbol{R}}_{LL,ji}^H(2\chi_{3,ju}\boldsymbol{I}_N\\ &+2\chi_{4,ju}\bar{\boldsymbol{G}}_{LR,ju}\bar{\boldsymbol{G}}_{LR,ju}^H)(\chi_{1,ji}\bar{\boldsymbol{h}}_{LL,ji}+\chi_{2,ji}\bar{\boldsymbol{R}}_{LL,ji}\boldsymbol{\phi}_i), \quad (39c)\\ \frac{\partial f_{6,juu}(\boldsymbol{\phi}_u)}{\partial\boldsymbol{\phi}_u}=&\,\Big\{\frac{\partial f_{6,jui}(\boldsymbol{\phi}_u,\boldsymbol{\phi}_i)}{\partial\boldsymbol{\phi}_u}+\frac{\partial f_{6,jui}(\boldsymbol{\phi}_u,\boldsymbol{\phi}_i)}{\partial\boldsymbol{\phi}_i}\Big\}\Big|_{i\to u}, \quad (39d)\\ \frac{\partial f_{7,juk}(\boldsymbol{\phi}_u)}{\partial\boldsymbol{\phi}_u}=&\\ &2\chi_{2,ju}\bar{\boldsymbol{R}}_{LL,ju}^H\big(a_{LG,jk}^2\boldsymbol{h}_{LG,jk}\boldsymbol{h}_{LG,jk}^H+b_{LG,jk}^2\boldsymbol{I}_N\big)\bar{\boldsymbol{R}}_{LL,ju}\boldsymbol{\phi}_u\\ &+2\chi_{1,ju}\big(a_{LG,jk}^2\boldsymbol{h}_{LG,jk}^H\bar{\boldsymbol{h}}_{LL,ju}+b_{LG,jk}^2\big)\bar{\boldsymbol{R}}_{LL,ju}^H\boldsymbol{h}_{LG,jk}, \quad (39e)\end{aligned}$$

where $(\cdot)\ |_i\ i\to u$ and $(\cdot)\ |_i\ i\leftrightarrow u$ denotes the operation of replaceing index u with i and replace them by each other in the expressions $(\cdot)$, respectvely. Similar to (19)-(22), the Riemannian gradient of $F_{MR}(\boldsymbol{\Phi}^{(l)})$ on the complex sphere manifold (33b) can be given by the projection of Euclidean gradient on the corresponding tangent space as follows

$$\begin{aligned}\text{Rgrad}_{\boldsymbol{\Phi}^{(l)}}F_{MR}(\boldsymbol{\Phi}^{(l)})=&\,\nabla F_{MR}(\boldsymbol{\Phi}^{(l)})\\ &-\text{Re}\big\{\nabla F_{MR}(\boldsymbol{\Phi}^{(l)})\odot(\boldsymbol{\Phi}^{(l)})^\dagger\big\}\odot\boldsymbol{\Phi}^{(l)}, \quad (40)\end{aligned}$$

Then, with a given cost function and gradient, an RGD or RCG algorithm can be implemented to solve the manifold optimization problem (P9). Finally, the optimal solution to (P8) can be obtained by updating $\boldsymbol{\Phi}$ and μ iteratively.

B. Overall Algorithm and Complexity Analysis

The overall two-stage algorithm is detailed in Algorithm 3. After initializing power allocation parameters without the aid of RISs, we optimize RIS phase shifts iteratively in Stage 1. Specifically, the RIS phase shifts can be obtained via the ES-SP-RMO algorithm with fixed μ. To guarantee the problem is solvable and the accuracy of the problem, we gradually reduce

$$\nabla F_{MR}\left(\boldsymbol{\Phi}\right)$$
$$= \Big(\sum_{u}\exp\left(-\mathrm{SINR}_{u}^{\mathrm{cCSI,MR,CF}}\left(\boldsymbol{\Phi}\right)/\mu\right)\Big)^{-1}\sum_{u}\exp\left(-\mathrm{SINR}_{u}^{\mathrm{cCSI,MR,CF}}\left(\boldsymbol{\Phi}\right)/\mu\right)\nabla\mathrm{SINR}_{u}^{\mathrm{cCSI,MR,CF}}\left(\boldsymbol{\Phi}\right)$$
$$- 2\sum_{k\in\mathcal{K}}\Big(\sum_{j\in\mathcal{J}}\sum_{u\in\mathcal{U}}p_{ju}f_{7,juk}\left(\boldsymbol{\phi}_{u}\right)-\varsigma_{k}\Big)\Big[\sum_{j\in\mathcal{J}}p_{j1}\frac{\partial f_{7,j1k}(\boldsymbol{\phi}_{1})}{\partial\boldsymbol{\phi}_{1}}\quad\cdots\quad\sum_{j\in\mathcal{J}}p_{jU}\frac{\partial f_{7,jUk}(\boldsymbol{\phi}_{U})}{\partial\boldsymbol{\phi}_{U}}\Big]_{U\times M} \tag{37}$$

$$\nabla\mathrm{SINR}_{u}^{\mathrm{cCSI,MR,CF}}\left(\boldsymbol{\Phi}\right)$$
$$= \Big(\sum_{j\in\mathcal{J}}\sum_{i\in\mathcal{U}}p_{ji}f_{6,jui}(\boldsymbol{\phi}_{u},\boldsymbol{\phi}_{i})-\sum_{j\in\mathcal{J}}p_{ju}f_{5,ju}(\boldsymbol{\phi}_{u})+f_{4}(\boldsymbol{\phi}_{u})+\sigma_{u}^{2}\Big)^{-2}\Big\{\Big(\sum_{j\in\mathcal{J}}\sum_{i\in\mathcal{U}}p_{ji}f_{6,jui}(\boldsymbol{\phi}_{u},\boldsymbol{\phi}_{i})+f_{4}(\boldsymbol{\phi}_{u})+\sigma_{u}^{2}\Big)$$
$$\times\Big[\mathbf{0}_{u-1}\ \ \sum_{j\in\mathcal{J}}p_{ju}\frac{\partial f_{5,ju}(\boldsymbol{\phi}_{u})}{\partial\boldsymbol{\phi}_{u}}\ \ \mathbf{0}_{U-u}\Big]_{U\times M}-\sum_{j\in\mathcal{J}}p_{ju}f_{5,ju}(\boldsymbol{\phi}_{u})\Big[\mathbf{0}_{u-1}\ \ \frac{\partial f_{4}(\boldsymbol{\phi}_{u})}{\partial\boldsymbol{\phi}_{u}}\ \ \mathbf{0}_{U-u}\Big]_{U\times M}-\sum_{j\in\mathcal{J}}p_{ju}f_{5,ju}(\boldsymbol{\phi}_{u})$$
$$\times\Big(\Big[\sum_{j\in\mathcal{J}}p_{j1}\frac{\partial f_{6,jui}(\boldsymbol{\phi}_{u},\boldsymbol{\phi}_{1})}{\partial\boldsymbol{\phi}_{1}}\ \ \cdots\ \ \sum_{j\in\mathcal{J}}p_{jU}\frac{\partial f_{6,jui}(\boldsymbol{\phi}_{u},\boldsymbol{\phi}_{U})}{\partial\boldsymbol{\phi}_{U}}\Big]_{U\times M}+\Big[\mathbf{0}_{u-1}\ \ \sum_{j\in\mathcal{J}}\sum_{i\in\mathcal{U},i\neq u}p_{ji}\frac{\partial f_{6,jui}(\boldsymbol{\phi}_{u},\boldsymbol{\phi}_{i})}{\partial\boldsymbol{\phi}_{u}}\ \ \mathbf{0}_{U-u}\Big]_{U\times M}\Big)\Big\} \tag{38}$$

Algorithm 3 Two-Stage Algorithm for (P6).

1: Initialize power allocation parameters $\boldsymbol{p}^{\mathrm{INIT}}$ under MR precoding without RISs via (P7) and (32) .

Stage 1: Optimizing phase shifts at RISs via ES-SP-RMO iterative algorithm in Section V-A.

2: Set iteration number of RGD or RCG $l_4 = 0$, set expotential smoothing parameter $\mu = \mu^{(0)}$. Solve (P9) for once via RGD or RCG with Riemannian gradient in (40); Solve (P7) for once to update $\boldsymbol{p}^{\mathrm{INIT}}$ for the next step.
3: **repeat**
4: Solve (P9) via RGD or RCG with $\mathrm{Rgrad}_{\boldsymbol{\Phi}^{(l_4)}}F_{MR}\left(\boldsymbol{\Phi}\right)$ in (40) and obtain $\boldsymbol{\Phi}^{(l_4+1)}$. Set $l_4 = l_4 + 1$.
5: **if** $F_{MR}(\boldsymbol{\Phi}^{(l_4)}) > F_{MR}(\boldsymbol{\Phi}^{(l_4-1)})$ **then**
6: $\boldsymbol{\Phi}^{*} = \boldsymbol{\Phi}^{(l_4)}$, $\mu^{(l_4)} = \mu^{(l_4-1)}$
7: **else** $\mu^{(l_4)} = \mu^{(l_4-1)}/2$.
8: **until** $\mu < \epsilon_{ES}$.

Output 1: The optimized RIS phase shifts matrix $\boldsymbol{\Phi}^{*}$.

Stage 2: Power Allocation via fractional programming with Given $\boldsymbol{\Phi}$ obtained from Stage 1.

9: Substituting the RIS phase shifts $\boldsymbol{\Phi} = \boldsymbol{\Phi}^{*}$ into (P7).
10: Performing the quadractic transform-based iterative algorithm as depicted from *line 2* to *line 6* in Algorithm 2.

Output 2: The optimized power allocation parameters $\boldsymbol{p}^{*}$.

μ to a sufficiently small value. The process is non-decreasing with guaranteed convergence [50],[51]. Then, in Stage 2, with Given RIS phase shifts, the power allocation subproblem can be solved by Algorithm 2. The computational complexity of Algorithm 3 is $\mathcal{O}(L_4(J^2U^2NM^2)+L_3(JN)^{3.5})$, where L_4 is the number of iterations in Stage 1. In each iteration of ES-SP-RMO, the complexity mainly originates from calculating the gradient (40).

VI. Extended Designs for Cooperative Beamforming Exploiting Two-Timescale CSI

Using pure statistical CSI in RIS-aided MIMO systems minimizes the overhead and delay from channel estimation but may lead to certain performance degradation. To mitigate this, the two-timescale transmission protocol is introduced to reduce the channel estimation overhead while preserving more performance [23], exploiting the statistical CSI for passive beamformers at RISs and the instantaneous superimposed CSI for active beamformers at satellites. In this section, we extend the proposed cooperative beamforming designs in the previous sections to accommodate two-timescale CSI for transmission.

A. Impact of Two-Timescale CSI for Active Beamformers

For the cooperative beamforming design under adaptive precoding in Section III, due to LUs only using statistical CSIs for SIC decoding, the objective function will not be changed with instantaneous superimposed CSI, according to (5). Thus, Algorithm 1 remains unchanged, and a two-timescale will not bring performance gain to this case. However, for cooperative beamforming designs under MR precoding, the instantaneous CSI at the satellite transmitter may bring performance gain because when the two-timescale CSI is available, the MR precoding can be written as (23), i.e., $\boldsymbol{w}_{ju}^{\mathrm{iCSI}} = \sqrt{p_{ju}}(\boldsymbol{h}_{LL,ju} + \boldsymbol{h}_{R,u}\boldsymbol{\Phi}_{u}\boldsymbol{G}_{LR,ju})$, instead of merely using channel statistics of LoS part as performed in (24). Then, this change will be incorporated into the RIS phase shift design.

Accordingly, we focus on cooperative beamforming under MR precoding and derive a series of modified closed-form expressions. By leveraging two-timescale CSIs, the RIS phase shifts optimization problem can be modified as

$$(\mathrm{P10}): \max_{\{\boldsymbol{\Phi}_{u}\}_{u=1}^{U},\boldsymbol{p}}\ \min_{\forall u\in\mathcal{U}}\ \left\{\mathrm{SINR}_{u}^{\mathrm{TTS,MR}}(\boldsymbol{\Phi})\right\} \tag{41a}$$
$$\text{s.t.}\sum_{j\in\mathcal{J}}\sum_{u\in\mathcal{U}}p_{ju}\mathbb{E}\left\{|\boldsymbol{h}_{LG,jk}^{H}(\boldsymbol{h}_{LL,ju}+\boldsymbol{G}_{LR,ju}\boldsymbol{\Phi}_{u}\boldsymbol{h}_{R,u})|^{2}\right\} \leq \varsigma_{k}, \forall k\in\mathcal{K}, \tag{41b}$$
$$\sum_{u\in\mathcal{U}}p_{ju}\mathbb{E}\left\{\|\boldsymbol{h}_{LL,ju}+\boldsymbol{h}_{R,u}\boldsymbol{\Phi}_{u}\boldsymbol{G}_{LR,ju}\|^{2}\right\}\leq P_{T}, \forall j\in\mathcal{J}, \tag{41c}$$
$$|\phi_{u,m}|^{2} = 1, \forall u\in\mathcal{U}, \forall m, \tag{41d}$$

where $\mathrm{SINR}_{u}^{\mathrm{TTS,MR}}(\boldsymbol{\Phi})$ is the function of $\boldsymbol{\Phi}$ involving two-timescale CSI, written in (42) at the top of next page.

$$\mathrm{SINR}_u^{\mathrm{TTS,MR}}(\boldsymbol{\Phi}) = \frac{\sum_{j=1}^{J} p_{ju}\left|\mathbb{E}\{\left\|\boldsymbol{h}_{L,ju}^H\right\|^2\}\right|^2}{\sum_{j\in\mathcal{J}}\sum_{i\in\mathcal{U},} p_{ji}\mathbb{E}\{\left|\boldsymbol{h}_{L,ju}^H\boldsymbol{h}_{L,ji}\right|^2\} - \sum_{j=1}^{J} p_{ju}\left|\mathbb{E}\{\left\|\boldsymbol{h}_{L,ju}^H\right\|^2\}\right|^2 + \mathbb{E}\{\left|h_{G,u}^H\right|^2\} + \sigma_u^2} \tag{42}$$

$$\mathrm{SINR}_u^{\mathrm{TTS,MR,CF}}(\boldsymbol{\Phi}) = \frac{\sum_{j=1}^{J} p_{ju} f_{8,ju}(\boldsymbol{\phi}_u)}{\sum_{j\in\mathcal{J}}\sum_{i\in\mathcal{U}} p_{ji} f_{9,jui}(\boldsymbol{\phi}_u,\boldsymbol{\phi}_i) - \sum_{j=1}^{J} p_{ju} f_{8,ju}(\boldsymbol{\phi}_u) + f_4(\boldsymbol{\phi}_u) + \sigma_u^2} \tag{44}$$

B. Closed-Form Expressions and Power Allocation

Similar to the procedures in Algorithm 2, (P10) can be solved by adopting RIS phase shifts obtained from Algorithm 1 and then performing power allocation. After the derivation of closed-form expressions, the problem is reformulated as

$$(\mathrm{P11}): \max_{\{\boldsymbol{\Phi}_u\}_{u=1}^U, \boldsymbol{p}} \min_{\forall u\in\mathcal{U}} \mathrm{SINR}_u^{\mathrm{TTS,MR,CF}}(\boldsymbol{\Phi}) \tag{43a}$$

$$\text{s.t.} \sum_{j\in\mathcal{J}}\sum_{u\in\mathcal{U}} p_{ju} f_{10,juk}(\boldsymbol{\phi}_u) - \varsigma_k \le 0, \forall k\in\mathcal{K}, \tag{43b}$$

$$\sum_{u\in\mathcal{U}} p_{ju}\sqrt{f_{8,ju}(\boldsymbol{\phi}_u)} - P_T \le 0, \forall j\in\mathcal{J}, \tag{43c}$$

$$|\phi_{u,m}|^2 = 1, \forall u\in\mathcal{U}, \forall m, \tag{43d}$$

where $\mathrm{SINR}_u^{\mathrm{TTS,MR,CF}}(\boldsymbol{\Phi})$ denotes the closed-form SINR expression in (44) at the top of next page, and we have

$$f_{8,ju}(\boldsymbol{\phi}_u) = (\mathrm{tr}\{\boldsymbol{\Xi}_{ju}\})^2 \tag{45a}$$

$$\begin{aligned} f_{9,jui}(\boldsymbol{\phi}_u,\boldsymbol{\phi}_i) &= f_{6,jui}(\boldsymbol{\phi}_u,\boldsymbol{\phi}_i) \\ &+ 2\chi_{1,ju}\chi_{4,ji}\mathrm{Re}\{\bar{\boldsymbol{h}}_{LL,ju}^H\bar{\boldsymbol{G}}_{LR,ji}\bar{\boldsymbol{G}}_{LR,ji}^H\bar{\boldsymbol{R}}_{LL,ju}\boldsymbol{\phi}_u\} + 2\chi_{1,ju} \\ &\times\chi_{3,ji}\mathrm{Re}\{\bar{\boldsymbol{h}}_{LL,ju}^H\bar{\boldsymbol{R}}_{LL,ju}\boldsymbol{\phi}_u\} + \chi_{4,ji}\chi_{2,ju}\|\boldsymbol{\phi}_u^H\bar{\boldsymbol{R}}_{LL,ju}^H\bar{\boldsymbol{G}}_{LR,ji}\|^2 \\ &+ \chi_{3,ji}\chi_{2,ju}\|\boldsymbol{\phi}_u^H\bar{\boldsymbol{R}}_{LL,ju}^H\|^2 + \alpha_{LL,ju}^2\chi_{4,ji}\|\bar{\boldsymbol{h}}_{LL,ju}^H\bar{\boldsymbol{G}}_{LR,ji}\|^2 \\ &+ \chi_{4,ji}\chi_{4,ju}\mathrm{tr}\{\bar{\boldsymbol{G}}_{LR,ji}\bar{\boldsymbol{G}}_{LR,ji}^H\bar{\boldsymbol{G}}_{LR,ju}\bar{\boldsymbol{G}}_{LR,ju}^H\} + \chi_{3,ji}\alpha_{LL,ju}^2 N \\ &+ \chi_{3,ji}\chi_{3,ju}N + \chi_{3,ju}\chi_{4,ji}MN + \chi_{3,ji}\chi_{4,ju}MN \end{aligned} \tag{45b}$$

$$\begin{aligned} f_{9,juu}(\boldsymbol{\phi}_u) &= \|\alpha_{LL,ju}\bar{\boldsymbol{h}}_{LL,ju} + \alpha_{LR,ju}\alpha_{R,u}\bar{\boldsymbol{R}}_{LL,ju}\boldsymbol{\phi}_u\|^4 + (\chi_{3,ju} \\ &+ \chi_{3,ju}N + 2\chi_{4,ju}NM)\|\alpha_{LL,ju}\bar{\boldsymbol{h}}_{LL,ju} + \alpha_{LR,ju}\alpha_{R,u}\bar{\boldsymbol{R}}_{LL,ju}\boldsymbol{\phi}_u\|^2 \\ &+ 2\chi_{4,ju}\|\bar{\boldsymbol{G}}_{LR,ju}^H(\alpha_{LL,ju}\bar{\boldsymbol{h}}_{LL,ju} + \alpha_{LR,ju}\alpha_{R,u}\bar{\boldsymbol{R}}_{LL,ju}\boldsymbol{\phi}_u)\|^2 \\ &+ 4N\chi_{6,ju}\mathrm{Re}\{\boldsymbol{\phi}_u^H\bar{\boldsymbol{R}}_{LL,ju}^H(\chi_{1,ju}\bar{\boldsymbol{h}}_{LL,ju} + \chi_{2,ju}\bar{\boldsymbol{R}}_{LL,ju}\boldsymbol{\phi}_u)\} \\ &+ \chi_{5,ju}\chi_{6,ju}M^2N + (2\chi_{5,ju}\chi_{6,ju} + \chi_{6,ju}^2 + 2\chi_{4,ju}\chi_{3,ju})MN^2 \\ &+ 2\chi_{4,ju}^2M^2N^2 + (\chi_{6,ju}^2 + 2\chi_{4,ju}\chi_{3,ju})MN + \chi_{3,ju}^2N(N+1) \end{aligned} \tag{45c}$$

$$\begin{aligned} f_{10,juk}(\boldsymbol{\phi}_u) &= f_{7,juk}(\boldsymbol{\phi}_u) + \mu_{LG,jk}\chi_{3,ju}N + \beta_{LG,jk}^2\chi_{4,ju}NM \\ &+ \alpha_{LG,jk}^2\chi_{4,ju}\|\boldsymbol{h}_{LG,jk}^H\bar{\boldsymbol{G}}_{LR,ju}\|^2 \end{aligned} \tag{45d}$$

with $\chi_{5,ju} = \beta_{LR,ju}^2\alpha_{R,u}^2$ and $\chi_{6,ju} = \beta_{LR,ju}^2\beta_{R,u}^2$. Then, with the given RIS phase shift obtained from Algorithm 1, we can perform power allocation optimization according to Algorithm 2 and here omitted for brevity.

C. ES-SP-RMO Algorithm and Two-Stage Design

Referred to as Section V-A, the RIS phase shift optimization problem is written into a manifold optimization problem (P11),

$$(\mathrm{P12}) \qquad \boldsymbol{\Phi}^* = \underset{|\phi_{u,m}|=1,\forall u,\forall m}{\arg\max} \; F_{TTS}(\boldsymbol{\Phi}) \tag{46}$$

where $F_{TTS}(\boldsymbol{\Phi})$ is a scalar-valued function with complex matrix variables, derived after exponential smoothing and adding the sum-square penalty as described in (33a), as follows

$$\begin{aligned} F_{TTS}(\boldsymbol{\Phi}) = &-\mu\log\sum_{u\in\mathcal{U}}\exp\left(-\mathrm{SINR}_u^{\mathrm{TTS,MR,CF}}(\boldsymbol{\Phi})/\mu\right) \\ &- \sum_{k\in\mathcal{K}}\Big(\sum_{j\in\mathcal{J}}\sum_{u\in\mathcal{U}} p_{ju} f_{10,juk}(\boldsymbol{\phi}_u) - \varsigma_k\Big)^2. \end{aligned} \tag{47}$$

Then, we can optimize RIS phase shifts via the ES-SP-RMO algorithm. Note that the gradient $\nabla F_{TTS}(\boldsymbol{\Phi})$ can be similarly obtained from (37) and (38) by replacing the partial derivative in (39a)-(39e) with $\frac{\partial f_{8,ju}(\boldsymbol{\phi}_u)}{\partial\boldsymbol{\phi}_u}$, $\frac{\partial f_{9,jui}(\boldsymbol{\phi}_u,\boldsymbol{\phi}_i)}{\partial\boldsymbol{\phi}_i}$, $\frac{\partial f_{9,jui}(\boldsymbol{\phi}_u,\boldsymbol{\phi}_i)}{\partial\boldsymbol{\phi}_u}$, $\frac{\partial f_{9,juu}(\boldsymbol{\phi}_u)}{\partial\boldsymbol{\phi}_u}$, and $\frac{\partial f_{10,juk}(\boldsymbol{\phi}_u)}{\partial\boldsymbol{\phi}_u}$, respectively, as follows

$$\begin{aligned} \frac{\partial f_{8,ju}(\boldsymbol{\phi}_u)}{\partial\boldsymbol{\phi}_u} &= 2\,\mathrm{tr}\{\boldsymbol{\Xi}_{ju}\}\big(\chi_{2,ju}\bar{\boldsymbol{R}}_{LL,ju}^H\bar{\boldsymbol{R}}_{LL,ju}\boldsymbol{\phi}_u \\ &\quad + \chi_{1,ju}\bar{\boldsymbol{R}}_{LL,ju}^H\bar{\boldsymbol{h}}_{LL,ju}\big) \end{aligned} \tag{48a}$$

$$\frac{\partial f_{9,jui}(\boldsymbol{\phi}_u,\boldsymbol{\phi}_i)}{\partial\boldsymbol{\phi}_i} = \frac{\partial f_{6,jui}(\boldsymbol{\phi}_u,\boldsymbol{\phi}_i)}{\partial\boldsymbol{\phi}_i} \tag{48b}$$

$$\frac{\partial f_{9,jui}(\boldsymbol{\phi}_u,\boldsymbol{\phi}_i)}{\partial\boldsymbol{\phi}_u} = \frac{\partial f_{9,jui}(\boldsymbol{\phi}_u,\boldsymbol{\phi}_i)}{\partial\boldsymbol{\phi}_u}\Big|_{i\leftrightarrow u} \tag{48c}$$

$$\begin{aligned} \frac{\partial f_{9,juu}(\boldsymbol{\phi}_u)}{\partial\boldsymbol{\phi}_u} &= \bar{\boldsymbol{R}}_{LL,ju}^H\big\{\big(4\chi_{4,ju}NM + 2\chi_{3,ju}N + 2\chi_{3,ju} \\ &+ 4\|\alpha_{LL,ju}\bar{\boldsymbol{h}}_{LL,ju} + \alpha_{LR,ju}\alpha_{R,u}\bar{\boldsymbol{R}}_{LL,ju}\boldsymbol{\phi}_u\|^2\big) + \big(4\chi_{4,ju} \\ &\times\bar{\boldsymbol{G}}_{LR,ju}\bar{\boldsymbol{G}}_{LR,ju}^H\big)\big\}\big(\chi_{2,ju}\bar{\boldsymbol{R}}_{LL,ju}\boldsymbol{\phi}_u + \chi_{1,ju}\bar{\boldsymbol{h}}_{LL,ju}\big) \\ &+ 4N\chi_{6,ju}\bar{\boldsymbol{R}}_{LL,ju}^H(\chi_{1,ju}\bar{\boldsymbol{h}}_{LL,ju} + 2\chi_{2,ju}\bar{\boldsymbol{R}}_{LL,ju}\boldsymbol{\phi}_u) \end{aligned} \tag{48d}$$

$$\frac{\partial f_{10,juk}(\boldsymbol{\phi}_u)}{\partial\boldsymbol{\phi}_u} = \frac{\partial f_{7,juk}(\boldsymbol{\phi}_u)}{\partial\boldsymbol{\phi}_u} \tag{48e}$$

Finally, we can design a two-stage algorithm similar to Algorithm 3 to obtain optimal RIS phase shifts and power allocation parameters sequentially, and the details are omitted for brevity.

TABLE I
SIMULATION PARAMETERS

Parameter	Value
Satellite orbit altitude	LEO 550 km; GEO 36000 km
Frequency band	Ku-band, $f_c = 12$ GHz
Number of LEO satellites and antennas	$N = 16$, $J = 3$
Number of LUs and GTs	$U = 2$, $K = 1$
Inter-system Interference threshold	$\varsigma_k \triangleq \varsigma = -12.2$ dB
Total beam power of LEO satellites	$P_T = 50$ W
Radiation pattern of GTs	From ITU [5],[6]
Noise power density	$k_B T_R B_W = -94$ dbm
Number of RIS subsurfaces	$M = 25$
Reflecting elements in a subsurface	100×100
Size of a reflecting element	0.01 m $\times$ 0.01 m
Distance between the RIS and LUs	$d_{RU} = 100$ m
Rician factor of terrestrial links	$\kappa_{R,u} \triangleq \kappa_R = 10$ dB
Rician factor of GEO satellite links	$\kappa_{GG}, \kappa_{GL}, \kappa_{GR} \triangleq \kappa_G = 30$dB
Rician factor of LEO satellite links	$\kappa_{LL}, \kappa_{LR}, \kappa_{LG} \triangleq \kappa_L = 20$dB

VII. SIMULATION RESULTS

In this section, we provide numerical results to evaluate the effectiveness of the proposed joint multi-satellite multi-RIS beamforming schemes for LEO SatCom with LEO-GEO intersystem interference mitigation. The simulations adhere to the setup outlined in Table I unless stated otherwise. In the modeled scenario, one of the LUs is co-located with the GT, and one of the LEO satellites is *in-line* with the GEO satellite located at $(0°\mathbf{N}, 100°\mathbf{E})$. According to ITU regulations, *in-line* interference is the most severe case of LEO-GEO intersystem interference, and $\varsigma_k \leq 12.2$ dB must be guaranteed. The other LUs are spaced $2°$ apart in either longitude or latitude on Earth, and LEO satellites are separated by a latitude spacing $2.5°$. The computation of distance-dependent large-scale path-loss coefficients takes into account the specific link distance, normalized noise power, and multibeam antenna radiation patterns. The simulation compares the following schemes:

1) **AP-AO**: The AO-based cooperative beamforming design exploiting pure statistical CSI with adaptive precoding, as detailed in Algorithm 1.
2) **MR-S-PA**: Following the RIS phase shift optimization from Algorithm 1, this scheme involves power allocation using Algorithm 2 with MR precoding under statistical CSI.
3) **MR-S-TS**: The two-stage design with MR precoding in Algorithm 3, including ES-SP-RMO and power allocation.
4) **MR-TTS-PA**: Using similar algorithm to scheme MR-S-PA, but exploiting two-timescale CSI.
5) **MR-TTS-TS**: Using similar algorithm to scheme MR-S-TS, but exploiting two-timescale CSI.
6) **AP-NoRIS**: Adaptive precoding via Algorithm 1 without the aid of RISs, which serves as an initialization for AP-AO.
7) **MR-S-NoRIS**: MR precoding via Algorithm 3 without the aid of RISs, which serves as an initialization for MR-S-TS.
8) **MR-TTS-NoRIS**: Similar to MR-S-NoRIS but exploting two-timescale CSI, served as a initialization for MR-TTS-TS.

Fig. 2 and Fig. 3 compare the minimum SINR γ of LUs in different schemes versus satellite transmit power under Rician factors $\kappa_N, \kappa_R = 0dB$ and $20dB$, respectively, corresponding to different scattering environments. As readily observed, all cooperative beamforming schemes outperform the schemes without the aid of RISs, and the minimum SINR maintains an increase with transmit power in the first half of curves. Nevertheless, several interesting observations are made. First,

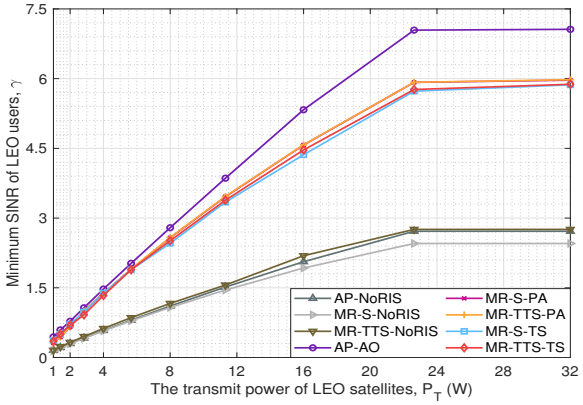

Fig. 2. Minimum SINR γ of LUs versus transmit power of LEO satellites P_T with the satellite-to-ground Rician factor $\kappa_N = 20\,dB$.

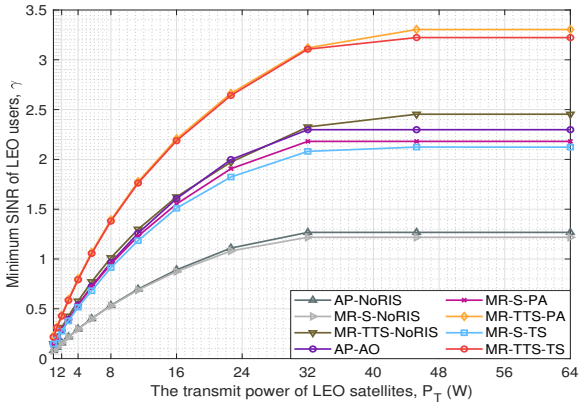

Fig. 3. Minimum SINR γ of LUs versus transmit power of LEO satellites P_T with the satellite-to-ground Rician factor $\kappa_N = 0\,dB$.

the SINR reaches its peak and no longer increases when P_T becomes sufficiently large, e.g., $P_T = 2^{4.5}W$. This phenomenon can be attributed to the LEO-GEO interference threshold, which restricts further performance enhancement with large P_T compared to the LEO satellite systems without spectrum sharing. Second, when $\kappa_N, \kappa_R = 20dB$, i.e., under a high Rician factor, the cooperative beamforming scheme AP-AO under adaptive precoding outperforms its MR precoding counterpart due to better intrasystem interference mitigation ability of adaptive precoding. However, when $\kappa_N, \kappa_R = 0dB$, the MR precoding schemes with two-timescale CSI even outperform AP-AO, which conforms to the theoretical expectation that MR-TT-PA and MR-TT-TS schemes effectively utilize instantaneous superimposed CSI at the transmitter.

Fig. 4 and Fig. 5 present γ versus LEO-GEO aggregation interference threshold ς under Rician factors $\kappa_N = 20dB, \kappa_R = 10dB$ and $\kappa_N = 0dB, \kappa_R = 10dB$, respectively. It can be observed that in scenarios with stronger LoS (Fig. 4), the performance is better than in weaker LoS scenarios (Fig. 5) because LoS-dominant means highly deterministic CSI for designing cooperative beamforming accurately. Interestingly, despite a fixed transmit power, γ improves as ς increases due to the relaxed LEO-GEO intersystem interference constraints that are easier to satisfy. Fig. 5 demonstrates that the performance gain of utilizing two-timescale CSIs persists. Besides, a notable distinction compared to Fig. 4 is the presence of a performance ceiling when ς is sufficiently large. This ceiling

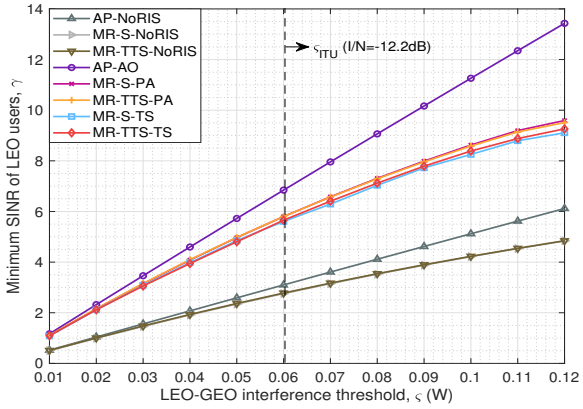

Fig. 4. Minimum SINR γ of LUs versus LEO-GEO interference threshold ς with the satellite-to-ground Rician factor $\kappa_N = 20\,dB$.

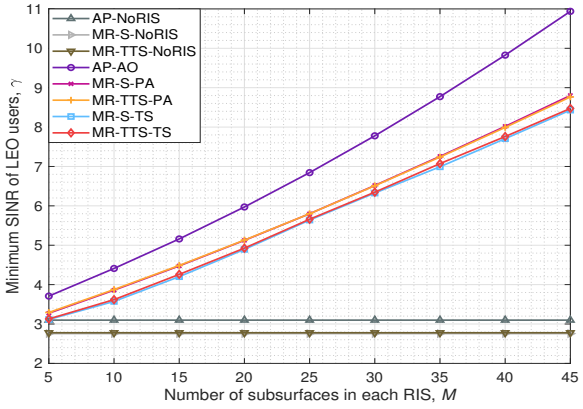

Fig. 6. Minimum SINR γ of LUs versus different number of RIS subsurfaces M with the satellite-to-ground Rician factor $\kappa_N = 20\,dB$.

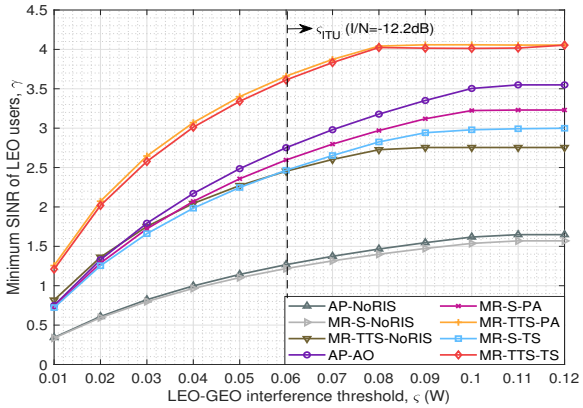

Fig. 5. Minimum SINR γ of LUs versus LEO-GEO interference threshold ς with the satellite-to-ground Rician factor $\kappa_N = 0\,dB$.

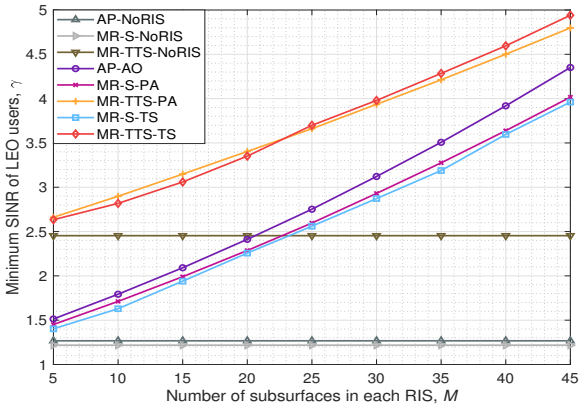

Fig. 7. Minimum SINR γ of LUs versus different number of RIS subsurfaces M with the satellite-to-ground Rician factor $\kappa_N = 0\,dB$.

reveals the maximum SINR achievable in an LEO SatCom system without implementing LEO-GEO interference mitigation strategies. Particularly in scenarios where the LoS component of the channels is weak, the statistical CSI-based transmission design experiences severe performance degradation.

Fig. 6 and Fig. 7 show the minimum SINR γ versus the number of RIS subsurfaces M. The findings indicate that a higher number of subsurfaces leads to improved SINR. The curve of the AP-AO scheme indicates the performance gain surpasses $\mathcal{O}(M)$ but does not reach the ideal power scaling law $\mathcal{O}(M^2)$ [18] due to the intersystem and intrasystem interference. For the MR precoding cases, the two-stage algorithm designs (MR-S-TS and MR-TTS-TS) closely match their respective power allocation counterparts (MR-S-PA and MR-TTS-PA) that use the RIS phase shifts results obtained from the adaptive precoding case, respectively, validating the effectiveness of the two-stage design. Again, lower Rician factors highlight the performance gain provided by two-timescale CSI. This gain can make the cooperative beamforming under MR precoding outperform its adaptive precoding counterpart.

In Fig. 8, Fig. 9, and Fig. 10, we present the impact of Rician factors on the system performance across different schemes. κ_R varies from $-12dB$ to $30dB$, and κ_N is set by $0dB$, $10dB$, and $20dB$ in each figure, respectively. It can be observed that the minimum SINR γ of LUs in all schemes increases when κ_N or κ_R increases. This is because a larger Rician factor reduces the uncertainty of CSIs when exploiting only the statistical CSI to design cooperative beamforming. The performance gradually stays stable around $\kappa_R = 15dB$. For a small κ_N regime, MR-TTS-PA and MR-TTS-TS using two-timescale SCI facilitate better beamforming gain. However, except for the small κ_N regime, AP-AO under adaptive precoding consistently yields higher gains, and the performance gap between adaptive and MR precoding widens as κ_N increases. The optimal scheme in practical scenarios should consider the signaling and channel estimation overhead of adaptive precoding and two-timescale CSI. For instance, the MR-TTS-TS scheme can be chosen for urban or forest scenarios with weak LoS propagation, the AP-AO scheme can be chosen for remote hotspot areas or emergency response with generally better performance, and MR-S-TS can be chosen for its practicality with relatively low overhead.

Fig. 11 compares the multi-satellite cooperation, denoted by 'MSC,' in a cell-free paradigm with a single-satellite transmission, denoted by 'SST,' in a centralized MIMO paradigm. We only plot AP-AO and MR-TTS-TS schemes with $\beta_N = 0dB$ and $20dB$ for clarity, where M-AP and M-MR denote MSC cases, and S-AP and S-MR denote SST cases using corresponding algorithms. In the SST cases, two LEO satellite positions are considered: one at a latitude $1.25°$ and the other at $2.5°$ away from the latitude of the GEO satellite. For a fair comparison, the same number of transmit antennas and transmit power in total is assumed. The results indicate that the performance of SST could outperform MSC when the

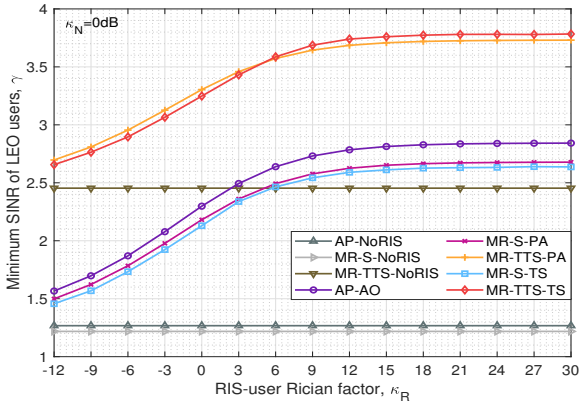

Fig. 8. Minimum SINR γ of LUs versus different terrestrial Rician factors κ_R and satellite-to-ground Rician factors (with $\kappa_N = 0\,dB$).

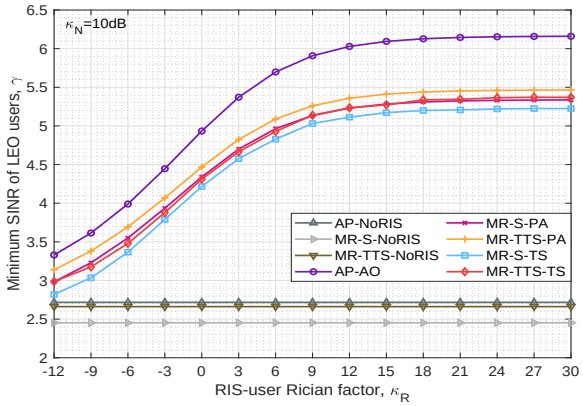

Fig. 9. Minimum SINR γ of LUs versus different terrestrial Rician factors κ_R and satellite-to-ground Rician factors (with $\kappa_N = 10\,dB$).

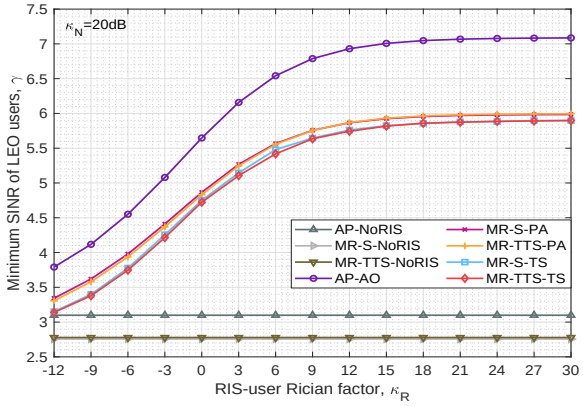

Fig. 10. Minimum SINR γ of LUs versus different terrestrial Rician factors κ_R and satellite-to-ground Rician factors (with $\kappa_N = 20\,dB$).

LEO satellite of SST is $2.5°$ away from GEO, attributed to its superior link budget and coherent beamforming gain. However, at closer proximity of $1.25°$, SST significantly underperforms MSC due to the loss of satellite diversity, which is essential for maintaining LEO SatCom performance while mitigating intersystem interference. In fact, in SST scenarios, if the LEO satellite is directly in line with the GEO satellite, the regulation on LEO-GEO interference mitigation may cause a malfunction in LEO SatCom. Therefore, with the increasing emphasis on intersystem interference avoidance, MSC has shown increasingly higher advantages than SST.

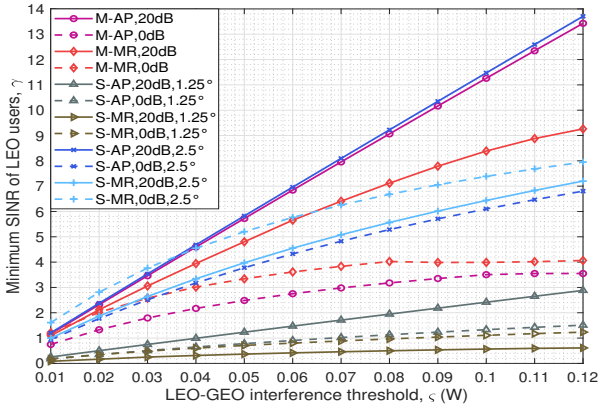

Fig. 11. Minimum SINR γ of LUs versus LEO-GEO interference threshold ς under multi-satellite cooperation and single-satellite transmission setups.

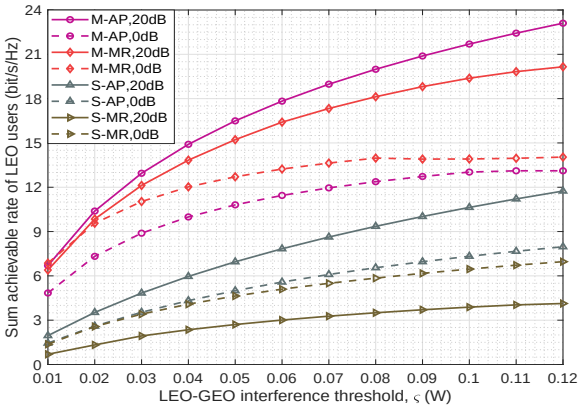

Fig. 12. Sum achievable rate of LUs versus LEO-GEO interference threshold ς under multi-satellite cooperation and single-satellite transmission setups.

Fig. 12 illustrates the sum achievable rate of LUs versus the LEO-GEO interference threshold under various MSC and SST setups in alignment with configurations in Fig. 11. The MSC (denoted by 'M-') consistently outperform the SST schemes (denoted by 'S-', $1.25°$ away from GEO) across all interference thresholds, demonstrating the performance gains through cooperative multi-satellite strategies. Both adaptive and MR precoding schemes show substantial improvements in sum rate with the increase in the LEO-GEO interference threshold. For SST cases, S-AP consistently outperforms S-MR, indicating its superior capability in bemforming optimizing. As for MST schemes, the performance gap between M-AP and M-MR can be inverse from high to low Rician factor, which highlights the importance of choosing effective precoding techniques in maximizing the achievable sum rate. Additionally, the sum rates under 20dB Rician factor are significantly higher than those under 0dB, suggesting that more accurate channel information amplify the benefits of cooperative transmission strategies.

Fig. 13 compares the total execution time and CPU running time of the proposed algorithms under various antenna and RIS subsurfaces configurations. The simulations were performed using MATLAB R2021a on an Intel(R) Core(TM) i7-10700K CPU @3.80GHz, with 32 GB RAM. The benchmark scheme AP-NoRIS shows relatively low execution and CPU running times across all configurations, as it incurs no additional computational cost for RIS passive beamforming. In contrast,

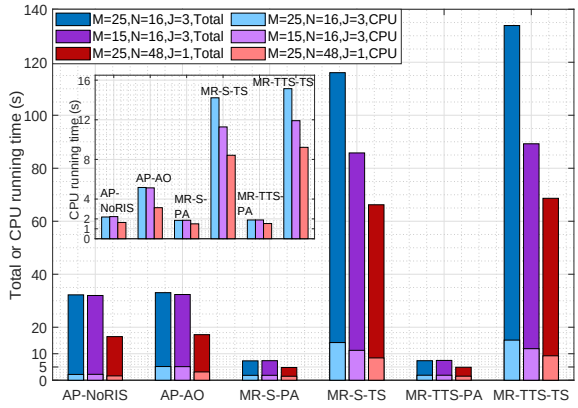

Fig. 13. The total execution time and CPU running time of the proposed algorithms with different antenna and RIS subsurfaces configurations (with $\kappa_N = 10\,dB$,$\kappa_R = 9\,dB$).

AP-AO has higher execution and CPU running times compared to AP-NoRIS, indicating better performance but at a higher computational cost. The power allocation algorithms MR-S-PA and MR-TTS-PA, based on AP-AO, exhibit moderate execution and CPU running times, making them practical choices for implementing MR precoding. However, MR-S-TS and MR-TTS-TS show notably higher execution and CPU running times, especially with larger values of M and N. While MR-TTS-TS offers potentially high performance, its high computational demands may limit its feasibility for real-time applications. Besides, the MSC strategies bring computational cost compare to its SST counterpart. To sum up, using adaptive precoding, less antennas and RIS elements, less cooperative LEO satellites, and power allocation schemes are prefered to reduce algorithm running time and improve practicality.

VIII. Conclusion

This paper investigated cooperative multi-satellite multi-RIS transmission to mitigate LEO-GEO intersystem interference while improving LEO SatCom. We proposed cooperative beamforming designs considering adaptive and MR precoding and statistical and two-timescale CSI within a non-coherent cell-free paradigm. These designs synthesized the advantages of cell-free and RIS into SatCom in a practical way. On leveraging pure statistical CSI, we first proposed an AO-based design with adaptive precoding, resorting to fractional programming and manifold optimization methods. Then, under MR precoding configuration, we derived closed-form expressions of optimization problems, following a power allocation-based design, and we developed the ES-SP-RMO algorithm to facilitate a two-stage design. We further extended closed-form expressions and proposed algorithms to leverage two-timescale CSI, which can balance the tradeoff between channel estimation overhead and SatCom performance. Simulation results validated the effectiveness of cooperative beamforming schemes in enhancing LEO SatCom and mitigating intersystem interference. Notably, the adaptive precoding case excelled in high Rician factor environments, while the MR precoding case effectively leveraged two-timescale CSI and performed better in low Rician scenarios. The results also highlighted the importance of multi-satellite diversity and the potential of RIS for SINR maintenance. Future work includes transmission designs when LUs use multiple antennas and distributed processing in multi-satellite multi-RIS cooperation systems.

Appendix A
Proof of the Downlink Equivalent SINR

Our proof follows the spirit of the results in [Lemma 2, 17], where multiple transmitters are operated non-coherently without synchronization. However, in our scenario, each satellite transmitter is equipped with multiple antennas, and these antennas are operated coherently with synchronization. Specifically, LUs detect the signal from LEO satellites sequentially by using the average channel $\mathbb{E}\{\boldsymbol{h}_{ju}^H\boldsymbol{w}_{ju}\}$ only. The received signal of LU u when detecting signal from j-th LEO satellite is

$$\begin{aligned} y_{ju} =& y_u - \sum_{i=1}^{j-1}\mathbb{E}\left\{\boldsymbol{h}_{iu}^H\boldsymbol{w}_{iu}\right\} && \text{(49a)}\\ =& \mathbb{E}\left\{\boldsymbol{h}_{ju}^H\boldsymbol{w}_{ju}\right\} + \left(\boldsymbol{h}_{ju}^H\boldsymbol{w}_{ju} - \mathbb{E}\left\{\boldsymbol{h}_{ju}^H\boldsymbol{w}_{ju}\right\}\right) \\ &+ \sum_{i=1}^{j-1}\left(\boldsymbol{h}_{iu}^H\boldsymbol{w}_{iu} - \mathbb{E}\left\{\boldsymbol{h}_{iu}^H\boldsymbol{w}_{iu}\right\}\right) + \sum_{i=j+1}^{J}\boldsymbol{h}_{iu}^H\boldsymbol{w}_{iu} \\ &+ \sum_{i=1}^{J}\sum_{v=1,v\neq u}^{U}\boldsymbol{h}_{iv}^H\boldsymbol{w}_{iv} + n_u && \text{(49b)} \end{aligned}$$

where (49a) derived from subtracting the previous $j-1$ signals. Only the first term in (49b) is the desired signal, while the ohter terms are regarded as uncorrelated noise ϖ_{ju} with power

$$\begin{aligned} &\mathbb{E}\{|\varpi_{ju}|^2\} \\ &= \sum_{i=1}^{J}\sum_{v=1}^{U}\mathbb{E}\{|\boldsymbol{h}_{iv}^H\boldsymbol{w}_{iv}|^2\} - \sum_{i=1}^{j}|\mathbb{E}\{\boldsymbol{h}_{iu}^H\boldsymbol{w}_{iu}\}|^2 + \sigma_u^2 \end{aligned} \quad (50)$$

Then, the total spectral efficiency of LU u can be expressed as $\mathrm{SE}_u = \sum_{i=1}^{J}\mathrm{SE}_{iu} = \log_2(\prod_{i=1}^{J}(1+\mathrm{SINR}_{iu}))$, where the inner term of logarithm function can be calculated as

$$\begin{aligned} \prod_{i=1}^{J}(1+\mathrm{SINR}_{iu}) &= \prod_{i=1}^{J}\left(1+\frac{|\mathbb{E}\{\boldsymbol{h}_{iu}^H\boldsymbol{w}_{iu}\}|^2}{\mathbb{E}\{|\varpi_{iu}|^2\}}\right) && \text{(51a)}\\ &= \prod_{i=1}^{J}\frac{\sum_{i=1}^{J}\sum_{v=1}^{U}\mathbb{E}\{|\boldsymbol{h}_{iv}^H\boldsymbol{w}_{iv}|^2\} - \sum_{i=1}^{j-1}|\mathbb{E}\{\boldsymbol{h}_{iu}^H\boldsymbol{w}_{iu}\}|^2 + \sigma_u^2}{\sum_{i=1}^{J}\sum_{v=1}^{U}\mathbb{E}\{|\boldsymbol{h}_{iv}^H\boldsymbol{w}_{iv}|^2\} - \sum_{i=1}^{j}|\mathbb{E}\{\boldsymbol{h}_{iu}^H\boldsymbol{w}_{iu}\}|^2 + \sigma_u^2} \\ &= \frac{\sum_{i=1}^{J}\sum_{v=1}^{U}\mathbb{E}\{|\boldsymbol{h}_{iv}^H\boldsymbol{w}_{iv}|^2\} + \sigma_u^2}{\sum_{i=1}^{J}\sum_{v=1}^{U}\mathbb{E}\{|\boldsymbol{h}_{iv}^H\boldsymbol{w}_{iv}|^2\} - \sum_{i=1}^{J}|\mathbb{E}\{\boldsymbol{h}_{iu}^H\boldsymbol{w}_{iu}\}|^2 + \sigma_u^2} && \text{(51b)} \end{aligned}$$

where the equivalent SINR of LU under non-coherent multi-satellite transmission can be written as (4).

References

[1] Z. Zheng, *et al.*, "RIS-aided LEO SatCom with LEO-GEO inter-system interference mitigation: joint multi-satellite multi-RIS beamforming", to be presented at *2024 IEEE Wireless Commun. Netw. Conf. (WCNC)*, Dubai, United Arab Emirates, 21-24 Apr. 2024.

[2] O. Kodheli, *et al.*, "Satellite communications in the new space era: a survey and future challenges," *IEEE Commun. Surveys Tuts.*, vol. 23, no. 1, pp. 70-109, 1st Quart., 2021.

[3] H. Al-Hraishawi, *et al.*, "A survey on nongeostationary satellite systems: the communication perspective," *IEEE Commun. Surveys Tuts.*, vol. 25, no. 1, pp. 101-132, 1st Quart., 2023.

[4] C. Braun, *et al.*, "Should we worry about interference in emerging dense NGSO satellite constellations?," in *Proc. IEEE Int. Symp. Dyn. Spectr. Access Netw (DySPAN)*, Newark, NJ, USA, 11-14 Nov. 2019.

[5] ITU, "Interference mitigation techniques to facilitate coordination between non-geostationary satellite orbit mobile-satellite service feeder links and geostationary-satellite orbit fixed-satellite service networks in the bands 19.3-19.7 GHz and 29.1-29.5 GHz," ITU-R S.1419, 1999.

[6] ITU, "Functional description to be used in developing software tools for determining conformity of non-geostationary-satellite orbit fixed-satellite service systems or networks with limits contained in Article 22 of the Radio Regulations," ITU-R S.1503-3, 2018.

[7] C. Zhang, *et al.*, "Spectrum sensing and recognition in satellite systems," *IEEE Trans. Veh. Technol.*, vol. 68, no. 3, pp. 2502-2516, 2019.

[8] S. K. Sharma, *et al.*, "In-line interference mitigation techniques for spectral coexistence of GEO and NGEO satellites," *Int. J. Satell. Commun. Netw.*, vol. 34, no. 1, pp. 11-39, 2016

[9] F. Zturk and A. Kara, "Exclusion zone minimization and optimal operational mode selection for co-existent geostationary and non-geostationary satellites," *Int. J. Satell. Commun. Netw.*, vol. 40, no. 3, pp. 191-203, 2022.

[10] Z. Xiao, *et al.*, "Guest editorial special issue on antenna array enabled space/air/ground communications and networking," *IEEE J. Sel. Areas Commun.*, vol. 40, no. 10, pp. 2767-2772, Oct. 2022.

[11] Z. Lin, *et al.*, "Multi-satellite beam hopping based on load balancing and interference avoidance for NGSO satellite communication systems," *IEEE Trans. Wireless Commun.*, vol. 71, no. 1, pp. 282-295, Jan. 2023.

[12] V. Joroughi, *et al.*, "Precoding in multigateway multibeam satellite systems," *IEEE Trans. Wireless Commun.*, vol. 15, no. 7, pp. 4944-4956, Jul. 2016.

[13] M. Khammassi, *et al.*, "Precoding for high throughput satellite communication systems: a survey," *IEEE Commun. Survey Tuts.*, early access, doi: 10.1109/COMST.2023.3316283.

[14] L. You, *et al.*, "Massive MIMO transmission for LEO satellite communications," *IEEE J. Sel. Areas Commun.*, vol. 38, no. 8, pp. 1851-1865, Aug. 2020.

[15] X. Zhang, *et al.*, "Multi-satellite cooperative networks: joint hybrid beamforming and user scheduling design," *IEEE Trans. Wireless Commun.*, early access, doi: 10.1109/TWC.2023.3346463.

[16] K. X. Li, Y. You, J. Wang, *et al.*, "Downlink transmit design for massive MIMO LEO satellite communications," *IEEE Trans. Commun.*, vol. 70, no. 2, pp. 1014-1028, Feb. 2022.

[17] Ö. Özdogan, *et al.*, "Performance of cell-free massive MIMO with rician fading and phase shifts," *IEEE Trans. on Wireless Commun.*, vol. 18, no. 11, pp. 5299-5315, Nov. 2019.

[18] M. Röper, *et al.*, "Beamspace MIMO forsatellite swarms," in *2022 IEEE Wireless Commun. & Netw. Conf. (WCNC)*, 2022, pp. 1307-1312.

[19] Z. Xiang, X. Gao, K. X. Li, *et al.*, "Massive MIMO downlink transmission for multiple LEO satellite communication," *IEEE Trans. Commun.*, 2024, early access.

[20] E. Björnson and L. Sanguinetti, "Making cell-free massive MIMO competitive with MMSE processing and centralized implementation," *IEEE Trans. Wireless Commun.*, vol. 19, no. 1, pp. 77-90, Jan. 2020.

[21] Q. Wu, *et al.*, "Intelligent reflecting surface-aided wireless communications: a tutorial," *IEEE Trans. Commun.*, vol. 69, no. 5, pp. 3313-3351, May 2021.

[22] Z. Zheng, *et al.*, "RIS-aided hotspot capacity enhancement for multibeam satellite systems," *IEEE Trans. Wireless Commun.*, vol. 23, no. 4, pp. 3648-3664, Apr. 2024.

[23] X. Gan, *et al.*, "Multiple RISs assisted cell-free networks with two-timescale CSI: performance analysis and system design," *IEEE Trans. Commun.*, vol. 70, no. 11, pp. 7696-7710, Nov. 2022.

[24] Y. Zhang, *et al.*, "Beyond cell-free MIMO: energy-efficient reconfigurable intelligent surface aided cell-free MIMO communications," *IEEE Trans. Cognit. Commun. Netw.*, vol. 7, no. 2, pp. 412-426, Jun. 2021.

[25] T. V. Nguyen, H. D. Le, *et al.*, "On the design of RIS-UAV relay-assisted hybrid FSO/RF satellite-aerial-ground integrated network," *IEEE Trans. Aero. Electron. Syst.*, vol. 59, no. 2, pp. 757-771, Apr. 2023.

[26] Q. Huang, *et al.*, "Joint resource and trajectory optimization in active IRS-Aided UAV relaying networks," *IEEE Trans. Wireless Commun.*, early access.

[27] K. Guo, and K. An, "On the performance of RIS-assisted integrated satellite-UAV-terrestrial networks with hardware impairments and interference," *IEEE Wireless Commun. Lett.*, vol. 11, no. 1, pp. 131-135, Jan. 2022.

[28] K. Tekbiyik, G. K. Kurt, A. R. Ekti, *et al.*, "Reconfigurable intelligent surfaces empowered THz communication in LEO satellite networks," *IEEE Access*, vol. 10, pp. 121957-121969, 2022.

[29] K. Tekbiyik, G. K. Kurt, and H. Yanikomeroglu, "Energy-efficient RIS-assisted satellites for IoT networks," *IEEE Internet of Things J.*, vol. 9, no. 16, pp. 14891-14898, Aug. 2022.

[30] Y. Ge, and J. Fan, "Active reconfigurable intelligent surface assisted secure and robust cooperative beamforming for cognitive satellite-terrestrial networks," *IEEE Trans. Veh. Technol.*, vol. 72, no. 3, pp. 4108-4113, Mar. 2023.

[31] T. M. Hoang, C. Xu, A. Vahid, *et al.*, "Secrecy-rate optimization of double RIS-aided space-ground networks," *IEEE Internet Things J.*, vol. 10, no. 15, pp. 13221-13234, Aug. 2023.

[32] J. Yuan, G. Chen, and M. Wen, *et al.*, "Secure transmission for THz-empowered RIS-assisted non-terrestrial networks," *IEEE Trans. Veh. Technol*, vol. 72, no. 5, pp. 5989-6000, May 2023.

[33] J. Xu *et al.*, "IRS-UAV assisted secure integrated sensing and communication," *IEEE Wireless Commun.*, early access.

[34] C. Wang, *et al.*, "Covert communications via two-way IRS with noise power uncertainty," *IEEE Trans. Commun*, early access.

[35] D. Song, Z. Yang, G. Pan, *et al.*, "RIS-assisted covert transmission in satellite-terrestrial communication systems," *IEEE Internet Things J.*, vol. 10, no. 22, pp. 19415-19426, Nov. 2023.

[36] Z. Lin, H. Niu, *et al.*, "Refracting RIS-aided hybrid satellite-terrestrial relay networks: joint beamforming design and optimization," *IEEE Trans. Aero. Electron. Syst.*, vol. 58, no. 4, pp. 3717-3724, Oct. 2022.

[37] X. Liu, B. Zhao, M. Lin, *et al.*, "IRS-aided uplink transmission scheme in integrated satellite-terrestrial networks," *IEEE Trans. Veh. Technol.*, vol. 72, no. 2, pp. 1847-1861, Feb. 2023.

[38] H. Dong, C. Hua, L. Liu, *et al.*, "Intelligent reflecting surface-aided integrated terrestrial-satellite networks," *IEEE Trans. Wireless Commun.*, vol. 22, no. 4, pp. 2507-2522, Apr. 2023.

[39] C. Pan, *et al.*, "An overview of signal processing techniques for RIS/IRS-aided wireless systems," *IEEE J. Sel. Topics Signal Process.*, vol. 16, no. 5, pp. 883-917, Aug. 2022.

[40] K. Zhi, C. Pan, H. Ren, *et al.*, "Power scaling law analysis and phase shift optimization of RIS-aided massive MIMO systems with statistical CSI," *IEEE Trans. Commun.*, vol. 70, no. 5, pp. 3558-3574, May 2022.

[41] X. Gan, C. Zhong, C. Huang, *et al.*, "RIS-assisted multi-user MISO communications exploiting statistical CSI," *IEEE Trans. Commun*, vol. 69, no. 10, pp. 6781-6792, Oct. 2021.

[42] C. Luo, X. Li, S. Jin, *et al.*, "Reconfigurable intelligent surface-assisted multi-cell MISO communication systems exploiting statistical CSI," *IEEE Wireless Commun. Lett.*, vol. 10, no. 10, pp. 2313-2317, Oct. 2021.

[43] M. M. Zhao, Q. Wu, *et al.*, "Intelligent reflecting surface enhanced wireless networks: two-timescale beamforming optimization," *IEEE Trans. Wireless Commun.*, vol. 20, no. 1, pp. 2-17, Jan. 2021.

[44] K. Liu, *et al.*, "Compact user-specific reconfigurable intelligent surfaces for uplink transmission," *IEEE Trans. Commun.*, vol. 70, no. 1, pp. 680-692, Jan. 2022.

[45] Z. Zhang, *et al.*, "Active RIS vs. passive RIS: which will prevail in 6G?," *IEEE Trans. Commun.*, vol. 71, no. 3, pp. 1707-1725, March 2023.

[46] K. Shen and W. Yu, "Fractional programming for communication systems—part I: power control and beamforming," *IEEE Trans. Signal Process.*, vol. 66, no. 10, pp. 2616-2630, May 15, 2018.

[47] M. Grant and S. Boyd. *CVX: MATLAB software for disciplined convex programming.* Accessed: 2016. [Online]. Available: http://cvxr.com/cvx

[48] N. Boumal, *et al.*, "Manopt, a Matlab toolbox for optimization on manifolds", *Journal of Machine Learning Research*, vol. 15, no. 42, pp. 1455-1459, 2014. Available: https://www.manopt.org

[49] E. Shtaiwi, *et al.*, "Sum-rate maximization for RIS-assisted integrated sensing and communication systems with manifold optimization," *IEEE Trans. Commun.*, vol. 71, no. 8, pp. 4909-4923, Aug. 2023.

[50] L. Zhou, *et al.*, "Coordinated multicell multicast beamforming based on manifold optimization," *IEEE Commun. Lett.*, vol. 21, no. 7, pp. 1673-1676, Jul. 2017.

[51] E. Polak, J. O. Royset, and R. S. Womersley, "Algorithms with adaptive smoothing for finite minimax problems," *J. Optim. Theory Appl.*, vol. 119, no. 3, pp. 459-484, Dec. 2003.